The calcium binding protein S100β marks hedgehog-responsive resident vascular stem cells within vascular lesions

¶Mariana Di Luca[1], ¶Emma Fitzpatrick[1], ¶Denise Burtenshaw[1], ¶Weimin Liu[2], Jay-Christian Helt[2], Roya Hakimjavadi[1], Eoin Corcoran[1], Yusof Gusti[1], Daniel Sheridan[1], Susan Harman[1], Catriona Lally[3], Eileen M. Redmond*[2] and Paul A. Cahill*[1]

[1] Dublin City University, Vascular Biology & Therapeutics Group, School of Biotechnology (Dublin, Ireland); [2] University of Rochester, Dept Surgery (Rochester, New York, United States) [3]Trinity College Dublin, Trinity Centre for Bioengineering, Trinity Biomedical Sciences Institute, (Dublin, Ireland).

¶ Contributed equally

* Both senior authors

Address for correspondence

Paul A. Cahill., BSc., PhD
Professor, School of Biotechnology
Chair of Vascular Biology & Therapeutics, School of Biotechnology
Lonsdale Bldg, Office X2-09, Faculty of Science and Health
Dublin City University, Glasnevin, Dublin 9. Ireland
E: paul.cahill@dcu.ie, Ph: 353-1-700-8466, Fax: 353-1-700-5412

Abstract

A hallmark of subclinical atherosclerosis is the accumulation of vascular smooth muscle cell (SMC)-like cells leading to intimal thickening. While medial SMCs contribute, the participation of hedgehog responsive resident vascular stem cells (vSCs) to lesion formation remains unclear. Using transgenic eGFP mice and genetic lineage tracing of S100β vSCs *in vivo*, we identified S100β/Sca1 cells derived from a S100β non-SMC parent population within lesions that co-localise with smooth muscle α-actin (SMA) cells following iatrogenic flow restriction, an effect attenuated following hedgehog inhibition with the smoothened inhibitor, cyclopamine. *In vitro*, S100β/Sca1 cells isolated from atheroprone regions of the mouse aorta expressed hedgehog signalling components, acquired the di-methylation of histone 3 lysine 4 (H3K4me2) stable SMC epigenetic mark at the Myh11 locus and underwent myogenic differentiation in response to recombinant sonic hedgehog (SHh). Both S100β and PTCH1 cells were present in human vessels while S100β cells were enriched in arteriosclerotic lesions. Recombinant SHh promoted myogenic differentiation of human induced pluripotent stem cell-derived S100β neuroectoderm progenitors *in vitro.* We conclude that hedgehog responsive S100β vSCs contribute to lesion formation and support targeting hedgehog signalling to treat subclinical arteriosclerosis.

Keywords: Arteriosclerosis, intimal thickening, resident vascular stem cells, S100β calcium binding proteins, stem cell antigen-1, lineage tracing, hedgehog signalling, human induced pluripotent stem cells (HiPSCs).

Introduction

Atherosclerosis is a chronic progressive inflammatory disease that leads to myocardial infarction and stroke [1]. Pathologic observations in humans vessels confirm that early 'transitional' lesions enriched with smooth muscle (SMC)-like cells called adaptive lesions are routinely present in atherosclerotic-prone regions of arteries before pathologic intimal thickening, lipid retention, and the appearance of a developed plaque [2]. Endothelial cell (EC) dysfunction due to disturbed blood flow is classically associated with the development of atheroprone lesions[3], while the embryological origin (e.g., neuroectoderm versus mesoderm) of SMCs may also influence disease localisation and progression[4]. These early lesions are routinely modelled in mouse carotid arteries following flow restriction[5] and can further rapidly develop into advanced atherosclerotic plaques in ApoE knockout on a Western diet [6,7].

Lineage tracing and single cell RNA sequence analysis (scRNA-seq) have provided compelling evidence in various animal models for the involvement of a rare population of (i) differentiated myosin heavy chain 11 (Myh11) medial SMC that are stem cell antigen-1 positive (Sca1^{+}) [8,9] and (ii) various adventitial and medial progenitors in progressing intimal thickening [10–13]. While some adventitial progenitors are derived from a parent Myh11 SMC population [14], non-SMC derived SRY-related HMG-box 10 (Sox10) adventitial/medial resident multipotent vascular stem cells (vSC), glioma-associated oncogene homolog 1 (Gli) and Nestin progenitor cells have also been implicated [13,15]. Despite these insights, the putative role of resident vSCs that do not originate from medial Myh11^{+} SMCs in promoting intimal thickening remains controversial.

S100β, a member of the S100 multigenic family expressing small (9 kDa and 14 kDa) Ca2+-binding proteins of the EF-hand type, is primarily localised to astrocytes and glial cells under normal physiological conditions and is positively associated with age and various neurodegenerative and neuroinflammatory diseases [16]. S100β promotes intimal thickening through interaction with the receptor for advanced glycation end-products (RAGE) [17] and induces migration and infiltration of inflammatory cells [18,19]. S100β plays a crucial role in maintaining an intermediate state of Sca1 progenitor cells following injury-induced neointimal thickening through a RAGE and stromal cell-derived factor-1 α/CXCR4 signalling mechanism [20].

Hedgehog signalling (Hh) is essential for normal embryonic development and plays a pivotal role in the maintenance of adult progenitor/stem cells in tissue repair after injury [21]. Hh signalling is initiated upon binding of a ligand to the canonical receptors, PTCH1 and PTCH2 (Patched 1 and 2) [22], which leads to disinhibition of SMO (Smoothened) and activation of a complex signalling cascade that regulates the GLI (glioma-associated oncogene homolog 1) family zinc finger transcription factors (GLI1, GLI2, and GLI3) [23]. GLI activators induce the transcription of Hh target genes primarily involved in cell proliferation, cell survival, and cell fate specification, including PTCH and GLI [24,25]. HHIP (hedgehog interacting protein) modulates hedgehog signalling activity by binding and inhibiting the action of hedgehog proteins [26]. Genome wide association studies (GWAS) in coronary artery disease patients have identified variants at the 14q32 HHIPL1 (Hedgehog interacting protein-like 1) that encode a paralog of HHIP [27] to increase Hh signalling and regulate SMC proliferation and migration *in vitro* [28]. In atherosclerotic mice, Hh has a permissive role through increased lipid uptake by macrophages [29], while global Hhipl1 deletion reduces plaque burden [28]. Hh signalling, especially SHh and signal peptide CUB domain and EGF like domain containing 2 (Scube2), are overexpressed in injured arteries during lesion formation after flow restriction [30–32], autogenous vein grafts [33], and hypoxic pulmonary arterial SMCs [34]. Adventitial Sca1^{+} cells that co-localise with SHh and Ptch1 [35] significantly contribute to intimal thickening *in vivo* [31,36,37] while Hh inhibition with cyclopamine or local perivascular depletion of Ptch1 attenuates intimal thickening following iatrogenic flow-restriction *in vivo* [38,39].

Given the pivotal role of Hh in the maintenance of adult progenitor/stem cells, tissue repair and atherosclerosis [21,28], we sought to determine the role of Hh responsive S100β/Sca1 vSCs and their myogenic progeny in contributing to intimal thickening and the progression of adaptive lesions *in vivo* and, furthermore, whether Hh signalling directs murine S100β vSCs and hiPSC-derived S100β neuroectoderm stem cells to undergo proliferation and myogenic differentiation *in vitro*.

Results

Perivascular Sca1 and S100β stem vSCs are present in normal adult vessels

The presence of perivascular Sca1 and S100β vSCs was first confirmed in whole mounted vessels from Sca1-eGFP and S100β-Cre-tdT mice. A discrete number of Sca1-eGFP and S100β-tdT cells were present on collagen fibres within the adventitial layer of the thoracic aorta, when compared to wild-type (WT) controls [Suppl Figure 1a-d]. The cells were located predominantly at the aortic arch and at bifurcations with intercostal vessels, and their presence diminished along the descending and abdominal aorta [Suppl Figure 1b, c]. When the media was removed, Sca1-eGFP cells were clearly present in adventitial layer of the thoracic aorta [Suppl Figure 1d] and in perivascular regions of the carotid artery [Suppl Figure 1d].

Sca1 and S100β cells are present in intimal lesions from murine carotid arteries following iatrogenic flow restriction.

The contribution of Sca1 cells to intimal medial thickening following iatrogenic flow restriction was first assessed in Sca1-eGFP transgenic mice following partial ligation of the left carotid artery (LCA). Vessels were harvested on day 3, 7 and 14 days post-ligation and paraformaldehyde fixed and paraffin-embedded cross sections were evaluated for eGFP (indicative of Sca1 expression) by confocal microscopy. Morphometric analysis confirmed that adventitial and intimal volumes increased significantly over time following ligation, without any significant change to medial volume, concomitant with a significant reduction in luminal volume after 7 and 14 days [Figure 1a].

The number of cells within the adventitial, medial and intimal layers of the LCA did not significantly change 3d post ligation [Figure 1b-d]. No Sca1- eGFP cells were visible within the medial layer of sham vessels which was populated primarily by α-smooth muscle actin (SMA) SMCs [Figure 1e]. While a small but significant number of Sca1-eGFP cells were present within the adventitial and intimal layers of sham vessels, the fraction of Sca1-eGFP cells significantly increased within the intimal layer 3d post ligation [Figure 1e, f]. Immunohistochemical analysis using anti-eGFP confirmed the presence of intimal Sca1-eGFP cells in ligated vessels [Figure 1e] and further demonstrated that intimal Sca1-GFP cells co-express PECAM-1/CD31 and endothelial cell nitric oxide (eNOS) [Figure 1e]. Moreover, there was also a notable

140 increase in the expression of the pro-apoptotic protein, Bax within the intimal, adventitial
141 and medial layer of the LCA and the medial layer of the RCA 3d post ligation [Figure 1g,h],
142 consistent with disturbed flow- and strain -induced apoptosis [40].

143 While the majority of Sca1-eGFP cells were present in the adventitial and intimal layers of
144 sham operated vessels, a small fraction were also visible within the medial layer after 7, 14
145 and 21d [Figure 2a, b and g and Suppl Figure 2a, b]. Upon injury, there was a notable
146 appearance of Sca1-eGFP cells within the expanding intimal layer of ligated vessels after 7, 14
147 and 21d [Figure 2a, b, d, g] that coincided with an increase in the number of cells [Figure 2c]
148 and the volume of the neointimal layer [Figure 1a]. Cumulative analysis revealed that there
149 was a significant increase in the fraction of Sca1-eGFP cells within neointimal layers after 7
150 and 14 and 21d, respectively, when compared to sham vessels or contralateral RCA [Figure
151 2d, h]. The majority of Sca1 cells within these lesions co-localised with SMA^+ cells [Figure 2e, f,
152 Suppl Figure 3a].

153 The contribution of S100β vSC to intimal thickening following iatrogenic flow restriction was
154 also assessed in S100β-eGFP transgenic mice. While the majority of S100β-eGFP cells were
155 present in the adventitial layer of sham operated vessels and the contralateral RCA, a small
156 fraction were also present within the medial layer after 21d [Suppl Figure 2a, c, Figure 2g, h].
157 In contrast, no intimal S100β-eGFP cells were present in sham vessels or the contralateral RCA
158 [Suppl Figure 2a c-e]. Upon injury, the fraction of S100β-eGFP cells within lesions significantly
159 increased when compared to sham vessels and the contralateral RCA [Suppl Figure 2d, e and
160 Figure 2 g,h]. Importantly, the number of double positive Sca1/S100β cells increased within
161 the neointimal layers of ligated vessels compared to the sham [Suppl Figure 2d, e] and
162 contralateral RCA control [Figure 2g, h]. Similarly, the number of double positive S100β/SMA
163 cells increased within lesions compared to the contralateral RCA [Figure 2i, j]. Taken together,
164 these data suggest double positive Sca1/S100β cells populate vascular lesions following
165 iatrogenic injury *in vivo*.

166 **Lineage tracing analysis of marked perivascular S100β cells iatrogenic flow restriction.**

167 In order to determine the source of intimal double positive Sca1/S100β cells following flow
168 restriction, lineage tracing analysis was performed using transgenic S100β-eGFP-CreERT2-
169 Rosa-26-tdTomato reporter mice [Suppl Figure 4a]. As cre-mediated recombination results in

170 a permanent heritable change in a cell's genome, these cells and their progeny remain
171 tdTomato (tdT) positive. The animals were treated with tamoxifen (Tm) for 7 days to induce
172 nuclear translocation of CreER(Tm) and subsequent recombination to indelibly mark S100β
173 cells with red fluorescent tdT seven days before ligation was performed [Suppl Figure 4b].
174 Only S100β cells present during the period of Tm treatment and their subsequent progeny
175 following injury are marked with tdT. The tissue specificity and recombination efficiency of
176 the Tm-induced Cre activity was confirmed in bone-marrow smears and neuronal tissue from
177 S100β-eGFP-CreERT2-Rosa-26-tdTomato mice. Treatment with Tm resulted in Cre-mediated
178 recombination and expression of S100β- tdT in >90% of neuronal cells of the carotid sinus
179 nerve (Hering's nerve) without any S100β-tdT cells observed in the bone marrow smears
180 [Suppl Figure 4c]. The neuronal staining was confirmed by immunohistochemical analysis of
181 S100β expression using both anti-S100β and anti-tdT antibodies (data not shown).

182 Morphometric analysis of the S100β-eGFP-creER2-Rosa26-tdT mice confirmed significant
183 intimal thickening in transgenic mice following ligation injury when compared to the sham
184 LCA and contralateral RCA [Figure 3a-c]. Treatment of S100β-eGFP-creER2-Rosa26-tdT
185 transgenic mice with tamoxifen indelibly marked S100β cells (S100β-tdT) within the
186 adventitial layer of the sham LCA prior to flow restriction [Figure 3d]. No cells are marked
187 when these double transgenic mice were treated with the vehicle control (corn oil) [Figure
188 3d]. Importantly, no S100β-tdT cells were observed in the intimal (EC) or medial (SMC) layers
189 of these sham vessels following tamoxifen treatment [Figure 3d]. However, following ligation,
190 there was a striking increase in the number of S100β-tdT marked cells within the medial and
191 intimal layers of the ligated LCA, compared to sham controls [Figure 3e, f]. In order to rule
192 out the possibility that Tm treatment continues to label a significant number of cells for
193 weeks after last Tm treatment [41], we confirmed that the fraction of S100β-tdT marked cells
194 remained significantly higher in the neointima of LCA four weeks after the last Tm injection
195 when compared to the RCA [Suppl Figure 4d, e]. Moreover, the fraction of S100β-tdT marked
196 cells within the LCA adventitial, medial and intimal layers of ligated vessels after one and four
197 weeks from the last Tm injection was of a similar magnitude [Suppl Figure 4f].

198 When S100β-tdT marked cells were evaluated for co-expression of Sca1 and SMA by
199 immunohistochemistry using anti-Sca1, anti-SMA and anti-tdT antibodies, S100β-tdT marked
200 cells co-localised with Sca1 cells in the adventitial and medial layers (but not the intimal layer)

201 of the control contralateral RCA before injury [Suppl Figure 3d, Figure 3g]. There was a
202 notable increase in the number of double stained Sca1/S100β-tdT cells in the media and
203 neointima of the LCA compared to the contralateral RCA [Figure 3g] and the sham LCA control
204 [Suppl Figure 3b] in double stained SMA/S100β-tdT cells within the neointima and media
205 compared to the sham control [Suppl Figure 3c]. Cumulative analysis confirmed both a
206 significant increase in the fraction of S100β-tdT cells [Figure 3h] and the fraction of double
207 stained S100β/Sca1 cells [Figure 3i] within the LCA medial and intimal layers compared to the
208 contralateral RCA control. Moreover, the majority of Sca1 cells within ligated vessels were
209 S100β-tdT cells [Figure 3j]. Since intimal and medial cells are not marked with tdT prior to
210 injury, these data suggest that these cells are derived from a non-SMC S100β parent
211 population following flow restriction. Moreover, the majority of intimal Sca1 cells are derived
212 from an S100β parent population.

213 **Hedgehog signalling components control intimal thickening following iatrogenic flow**
214 **restriction**

215 The effect of systemic administration of the Hedgehog inhibitor cyclopamine (10 mg/kg, IP,
216 every other day) on neointimal thickening and the accumulation of Sca1-eGFP cells was
217 evaluated. 2-hydroxypropyl-β-cyclodextrin (HβCD) was used as a vehicle control. Vessels
218 were harvested 7 and 14 d post-ligation and morphometric analysis was performed. Whole
219 vessel *Gli1 a*nd *Gli2* mRNA levels were significantly elevated in ligated vessels treated with
220 HβCD when compared to sham controls (Gli1: 6.1 ± 1.3 after 3 d; Gli2:8.1 ± 0.9 fold after 14d,
221 $p \leq 0.05$ n=4), an effect that was significantly reduced following cyclopamine treatment (Gli2:
222 3.2 ± 0.3 fold, n=4, $p \leq 0.05$). Immunohistochemical analysis revealed that the Hh receptor,
223 Ptch1, was up-regulated in LCA following injury concomitant with enhanced Gli2 expression in
224 LCA when compared to sham vessels [Figure 4a]. Gli2 co-localised with Sca1-eGFP expressing
225 cells and was markedly increased in ligated vessels treated with vehicle (HβCD) when
226 compared to sham-operated vessels, especially in the neointima and media of the LCA, an
227 effect that was attenuated following Hh inhibition [Figure 4a]. Cyclopamine treatment
228 significantly reduced the fraction of Sca1-eGFP expressing cells [Figure 4b, c] concomitant
229 with reduced intimal thickening 7 d and 14 d-post ligation [Figure 4d-g]. Collectively, these
230 data suggest that intimal thickening is attenuated by systemic administration of the

231 smoothened inhibitor, cyclopamine, concomitant with a reduction in the accumulation of
232 Gli2/Sca1 Hh-responsive cells within the intimal and medial layers.

233

234 **Isolation and characterisation of resident S100β/Sca1 vascular stem cells from murine**
235 **aorta**.

236 The expression of SMC differentiation markers genes, *Myh11* and *Cnn1* was enriched in
237 medial segments from both atheroprone aortic arch (AA) and atheroresistant
238 thoracic/abdominal aorta (TA) regions of the mouse aorta, when compared to NE-4C cells and
239 immortalised MOVAS mSMCs in culture [Figure 5a]. The level of S100β and Sox10 expression,
240 both markers of resident vascular stem cells [12,42], was then assessed in AA and TA regions,
241 with or without the adventitia [Figure 5b, c]. There was significant enrichment of both S100β
242 and Sox10 in the AA when compared to the TA. Moreover, the levels were significantly
243 enriched within the adventitia since its removal resulted in a dramatic reduction in the
244 expression of both transcripts. Nevertheless, medial expression of both genes was still
245 observed in the AA region [Figure 5b, c].

246 Resident vascular stem cells (vSCs) were subsequently isolated from mouse aortic arch (AA)
247 and thoracic aorta (TA) by enzymatic digestion and sequential plating, and were characterised
248 by flow cytometry, immunocytochemistry and gene expression for both stem cell markers and
249 SMC differentiation markers. Flow cytometric analysis confirmed that the cells were Sca1 and
250 S100β positive when compared to Sca1 and S100β positive control cell lines (i.e., C3H 10T1/2
251 and NE-4C, respectively) [Figure 5d]. The vSCs did not enrich for *Myh11* or *Cnn1* transcripts
252 when compared to fresh aortic tissue [Figure 5e, f] or express these proteins [Figure 5g,h] but
253 exhibited greater teleomere length as a measure of stemness when compared to freshly
254 isolated aortic SMC and to the immortalised MOVAS SMCs in culture [Figure 5i].
255 Immunocytochemical analysis revealed that vSCs from both AA and TA regions were Sca1
256 positive and expressed neuroectodermal markers S100β, Sox10, Sox17, and Nestin but were
257 negative for SMC differentiation markers *Cnn1* and *Myh11* [Figure 5g, h]. The vSCs were
258 enriched for neuroectodermal marker genes *S100β, Sox10 and Nestin* [Suppl Figure 5a-c], but
259 not for mesoderm markers *Kdr, Pax1 and Tbx6* [Suppl Figure 5d-f], when compared to SMCs
260 and NE-4 cells in culture. Collectively, these data indicate that neuroectodermal S100β/Sca1

261 cells are primarily located within the adventitial perivascular region of atheroprone regions of
262 the mouse aorta and can be isolated and expanded *in vitro* to retain these phenotypic
263 markers.

264 **Hedgehog signalling promotes myogenic differentiation of resident murine S100β/Sca1**
265 **vascular stem cells *in vitro.***

266 The functional effect of sonic hedgehog (SHh) signalling on the growth and myogenic
267 differentiation of vSCs was evaluated *in vitro* using multipotent Sca1/S100β cells isolated from
268 mouse aorta. Whole vessel Gli1 mRNA levels increased over time following ligation [Suppl
269 Figure 6c]. Treatment of vSCs isolated from AA and TA with recombinant SHh (rSHh, 0.5
270 µg/ml, 24h) promoted Hh signalling by increasing Hh target gene mRNA levels (*Gli 1*, *Gli 2* and
271 *Ptch1*), an effect blocked following pre-treatment with cyclopamine [Figure 5j, k and Suppl
272 Figure 6a, b]. Concurrent treatment of cells with rSHh for 7 days resulted in a significant
273 increase in SMC differentiation marker gene expression (*Cnn1* and *Myh11*), an effect
274 attenuated by pre-treatment of cells with cyclopamine [Figure 5j, k]. SHh treatment also
275 significantly increased the growth of AA vSCs after 7 days, an effect attenuated by pre-
276 treatment with cyclopamine [Suppl Figure 6d].

277 The level of enrichment of the SMC specific epigenetic histone mark, di-methylation of lysine
278 4 on histone H3 (H3K4me2) and the repressor mark, tri-methylation of lysine 27 on histone
279 H3 (H3K27me3) at the *Myh11* locus was assessed using chromatin immunoprecipitation
280 (ChIP) assays before and after rSHh treatment. Freshly isolated differentiated aortic medial
281 SMC and murine embryonic stem cells (mESCs) were used as positive/negative controls for
282 each mark and were markedly enriched for H3K4me2 and H3K27me3 at the Myh11 promoter,
283 respectively [Figure 5l-n]. In contrast to medial SMCs, AA vSCs were enriched for H3K27me3
284 but lacked enrichment of H3K4me2 at this locus. Treatment with recombinant SHh (rSHh, 0.5
285 µg/ml, 7d) increased the enrichment levels of the H3K4me2 mark while concurrently
286 decreasing the enrichment of the H3K27me3 mark, an effect attenuated by cyclopamine
287 [Figure 5l-n]. Finally, SHh treatment significantly increased the fraction of $Cnn1^{+}$ and $Myh11^{+}$
288 cells in AA vSCs, an effect attenuated by pre-treatment with cyclopamine [Figure 5o,p].

289 **S100β cells populate human arteriosclerotic lesions**

The expression of SMA, S100β and the hedgehog receptor, PTCH1, was determined by immunofluorescence staining in normal and arteriosclerotic human aortic sections. The expression of SMA was abundant in the medial layers of both normal and arteriosclerotic vessels while reduced within the neointima [Figure 6a]. The expression of S100β was confined to the adventitial layer of normal vessels but was significantly enhanced within the adventitial and intimal layers of arteriosclerotic sections [Figure 6a]. The expression of PTCH1 was confined to the adventitial layers of normal vessels but was also sparsely expressed in the medial and intimal layers of arteriosclerotic sections [Figure 6a].

Hedgehog signalling promotes myogenic differentiation of human induced pluripotent stem cell (HiPSC)-derived neuroectodermal S100β vascular stem cells *in vitro.*

To address whether human neuroectoderm S100β progenitors (NEPs) respond to hSHh by undergoing myogenic differentiation, S100β NEPs were isolated from human induced pluripotent stem cells (HiPSC) using a chemically defined protocol [43]. Human iPSCs enriched for Oct4 were treated with neuroectodermal inductive stimuli (FGF-2 and the selective inhibitor of ALK5, SB413642) for 7 days [Figure 6b] and expressed S100β but not SMC differentiation markers CNN1 and MYH11 [Figure 6b]. Treatment of NEPs with myogenic media supplemented with TGF-β1/PDGF-BB significantly increased the fraction of CNN1 and MYH11 cells after a further 12 d in culture, while concomitantly decreasing the number of S100β cells [Figure 6c]. The levels of S100β, CNN1 and MYH11 transcripts mirrored the changes in protein, where NEP-derived SMCs became significantly enriched for CNN1 and MYH11 following TGF-β1/PDGF-BB treatment as they diminish their expression of S100β [Figure 6d]. Treatment of NEPs with rSHh (1.0 µg/ml) for 12 d resulted in a significant increase in CNN1 and MYH11 mRNA levels, an effect attenuated by cyclopamine [Figure 6e, f], concomitant with an increase in the number of CNN1 positive cells [Figure 6g]. SHh treatment also significantly increased the growth of S100β NEPs after 12 days in culture, an effect attenuated by pre-treatment with cyclopamine [Suppl Figure 6e].

Discussion

In this study, we used transgenic mice and genetic lineage tracing approaches to delineate the involvement of Hh-responsive S100β resident vSCs in progressing neointima formation following flow restriction. Our findings indicate that intimal thickening involves significant accumulation of Hh-responsive S100β-derived progeny. Elucidation of this new cellular S100β source for generating SMC-like cells following injury expands our current understanding of vascular pathology and may represent an important therapeutic strategy for combating subclinical atherosclerosis.

SMC-like cells within neointimal lesions reportedly are monoclonal/oligoclonal in origin arising from the expansion of a pre-existing resident clonal population of cells [44–47]. Despite extensive research, their origin has remained controversial [48]. As a general rule, SMCs are purported to switch from a contractile phenotype to a less mature synthetic phenotype following vascular injury resulting in the loss of expression of SMC differentiation contractile markers, increased proliferation, and the synthesis and release of pro-inflammatory cytokines, chemotaxis-associated molecules, and growth factors [49]. However, whether these clonal progeny within lesions are derived primarily from differentiated medial SMCs [8,9,49], endothelial cells [10,50], and/or resident vSCs[10–13] remains unclear. Over the last decade, vascular SMC lineage tracing studies have provided compelling evidence of a significant role for pre-existing medial SMCs in vascular pathologies [8,51–53]. Single cell RNA sequence analysis (scRNA-seq) further identified a rare Sca1^{+} Myh11-Cre marked SMC subpopulation that gives rise to functionally distinct neointimal cells during lesion progression in mice [8,9]. However, although the Myh11-CreERT2 transgene was originally deemed specific for vascular SMC [54], data indicating expression of this and other 'SMC differentiation genes' in non-SMC populations has recently emerged [55–57] raising the possibility that other resident cells may be inadvertently marked and contribute to lesion formation. Myh11-CreER SMC lineage tracing studies have also demonstrated that the fraction of SMCs originating from pre-existing SMCs may be considerably smaller after severe transmural injury in mice further suggesting a contributory role for cells other than medial SMCs [58].

In this study, we provide genetic evidence that vascular lesions contain an abundance of dual labelled Hh responsive S100β/Sca1 vSCs derived from a non-SMC perivascular and/or medial S100β parent population. Notwithstanding the fact that Sca1 cells are present in bone-

marrow [59], bone-marrow cells were not marked using the S100β-CreERT2-tdT. It is therefore most likely that Sca1/S100β cells marked with S100β-CreERT2-tdT within lesions were locally derived [47]. S100β cells predominate within the adventitial layer of healthy vessels (murine and human) since removal of the adventitia dramatically reduced aortic S100β transcript levels in mice. Nevertheless, a small fraction of S100β/Sca1$^+$ cells are present in medial layer of normal vessels and could be successfully isolated from aortic medial segments following enzymatic digestion and sequential plating *in vitro*. Indeed, previous studies using *in situ* immunohistochemical analysis and scRNAseq also confirms the presence of a sparse Sox10/S100β cell population within the media, in addition to the adventitia [9,60,61]. However, these enrichment levels were minimal compared to an S100β$^+$ neuronal cell and vascular adventitial 'fibroblast-like cell' phenotypes within the vessel wall, supporting the contention that a perivascular adventitial S100β cell may be the predominant source of S100β within the vessel wall. Similarly, a discrete population of immature medial cells expressing CD146 that emerge during embryonic development may also contribute to neointimal formation in response to injury [58]. Whether these CD146 immature SMC progenitors are also S100β/Sca1 remains unclear although S100β vSCs derived from rat and murine aortic explants express CD146 [12,42]. In the future, it will be important to determine whether medial S100β vSCs differ from CD146 [58] and Myh11-CreER Sca1 cells [9] in their propensity to modulate different phenotypes and undergo clonal expansion using various injury models.

Adventitial progenitors have long been implicated in the progression of neointimal lesions following various vascular injuries [66,67]. However, in the absence of Sca1 or c-kit$^+$ stem cell lineage tracing experiments *in vivo*, the hypothesis of a regenerative function for adventitial Sca1 or c-kit$^+$ vSCs in lesion formation has been difficult to prove until recently. While perivascular cells must first traverse the internal and external elastic lamina to accumulate within the intima following injury [64], disruption of the elastic lamellae and flow-dependent enlargement of fenestrae can facilitate such migration [65–67]. Cell fate mapping studies have now clarified the role for adventitial PDGFR Sca1 progenitors in lesion progression following severe injury [11] while c-kit progenitors minimally facilitate endothelial regeneration or SMC differentiation to SMCs [68]. As Sca1-CreER marked cells were not present in vascular lesions following wire-induced injury [11], the origin of Sca1 neointimal cells following flow restriction in the current study is unlikely to be from a Sca1 parent population despite expressing Sca1

380 (albeit using a different injury model). Indeed, the percentage of perivascular S100β-CreER
381 marked cells that were Sca1^{+} in normal vessels was < 50% indicating that a Sca1^{neg}/S100β^{pos}
382 population might be responsible. In this context, S100β has been shown to maintain an
383 intermediate state of Sca1 progenitor cells following lesion formation[20]. Alternatively, this
384 residual Sca1^{pos}/S100β^{neg} population of adventitial Sca1 cells might represent Sca1 cells
385 derived from differentiated Myh11-CreER SMCs that expand in number following injury and
386 contribute to adventitial remodelling[14] and lesion formation [9]. While Sca1/S100β cells were
387 predominantly found in the developing intimal layer after 7, 14 and 21 days, these cells were
388 also present in the medial layer following injury. In agreement with previous studies
389 demonstrating significant apoptosis of medial SMCs following flow restriction[69], the
390 appearance of medial Sca1/S100β cells marked with S100β-CreERT2-tdT following early
391 expression of the pro-apoptotic protein Bax within the media is consistent with regeneration
392 of medial SMCs following injury.

393 Previous lineage tracing studies have also implicated endothelial cells (EC) that undergo
394 endothelial-to-mesenchymal transition (EndMT) to SMC-like cells as contributing to
395 neointimal formation during vein graft remodelling [10,50]. EndMT promotes neointimal
396 hyperplasia and induces atherogenic differentiation of EC [70]. In the current study, EC were not
397 marked with S100β-CreERT2-tdT prior to flow restriction suggesting that the S100β-CreERT2-
398 tdT marked cells within lesions do not originate from an EC parent population. These
399 apparent differences may result from the use of different models of vascular injury where
400 vein graft and atherosclerosis models involve different biomechanical stimuli and/or a
401 different inflammatory environments compared to the flow restriction model [50,71]. While EC
402 did not contribute to neointimal formation in developed lesions, a potential role for adluminal
403 Sca1 cells in regenerating the endothelium following ligation was observed. As flow restriction
404 leading to alterations in shear stress and cyclic strain is strongly associated with increased
405 endothelial cell apoptosis *in vitro* [72] and *in vivo* [73], significant Bax expression at the adluminal
406 surface was observed after flow restriction. Bcl-2/Bax ratios are an important rheostat to
407 determine the incidence of apoptosis in general and increases in Bax expression have been
408 widely reported and validated using the TUNNEL assay to indicate apoptosis of endothelial
409 cells *in vitro* in response to low shear stress (LSS) [74] and *in vivo* following carotid artery ligation
410 in wildtype mice [75] or following flow perturbation in ApoE deficient mice [76]. The increase in

Bax expression concomitant with an increase in the number of Sca1 cells that maintain a CD31 and eNOS endothelial cell phenotype at the adluminal surface is consistent with the appearance of new endothelial cells in the injured vessel that are derived from the proliferation of adluminal Sca1 cells. Indeed, recent cell fate mapping studies using Sca1-Cre-ERT2-tdT mice have since confirmed this observation by demonstrating expansion of Sca1-CreERT marked cells in the intimal layer that maintain CDH5 endothelial cell fate following injury [11].

There are many potential reasons for the different outcomes of lineage tracing studies that addressed the origin of lesional SMC-like cells including technical considerations around fixation, tissue preservation, brightness and contrast settings for image acquisition, autofluorescent material such as lipofuscin and single cell resolution [77]. Another important reason may involve the use of tamoxifen (Tm) in time-sensitive Tm-dependent Cre-LoxP models. Tm-induced Cre recombinase has been shown to indelibly mark cells up to 4 weeks after the last Tm injection thereby potentially confounding the interpretation of many previous studies [41]. In this context, we found that the fraction of S100β-CreER (tdT) marked cells within the various compartments of ligated vessels four weeks after the last Tm injection was similar to that observed after one week, indicating that, at least in our hands, medial SMC that might undergo de-differentiation and acquire the S100β promoter are not being inadvertently marked after injury.

Several GWAS studies have implicated HHIPL1 at the chromosome 14q32 CAD locus [27,78] and identified it as a secreted Hh signaling protein that modulates atherosclerosis-relevant vascular phenotypes [28]. Here we provide direct evidence that inhibition of Hh signalling controls neointimal thickening following flow restriction by attenuating the volume and accumulation of Sca1 cells within lesions. Furthermore, Hh signalling directly promotes Sca1/S100β cells from mouse and S100β neuroectoderm stem cells derived from human induced pluripotent stem cells (HiPSC) to undergo growth and myogenic differentiation to SMC-like cells *in vitro*. The possibility that Hh responsive S100β/Sca1 cells isolated from murine AA and TA regions are derived from a Myh11 medial SMC population was ruled out by examining the H3K4me2 epigenetic profile of S100β/Sca1 cells at the Myh11 locus, which is preserved during SMC phenotypic modulation *in vitro* and *in vivo* following injury[79]. Hh responsive S100β/Sca1 vSCs do not have this SMC histone mark and only become enriched

following myogenic differentiation to SMC-like cells, an effect attenuated by the Hh inhibitor, cylopamine. The accumulation of Sca1/S100β cells within lesions may be due, in part, to asymmetric division of Sca1/S100β progenitor stem cells (from the adventitia and/or media) and subsequent proliferation and migration of their partially differentiated myogenic progeny to the intima. Indeed, SHh promotes Sca1/S100β growth and the proliferation of modulated, partially differentiated SMCs *in vitro* [32]. Moreover, previous studies have shown that it is a Sca1 adventitial population in particular that proliferate following injury using immunohistochemical co-staining with Ki-67 [31]. This is not surprising as adventitial Sca1 stem cells co-localise with SHh and its receptor, Ptch1 [35] while several previous studies support a role for Hh signalling in vascular lesion formation in mice [29,38,39]. It appears the Yes-Associated Protein (YAP) is required for incorporation and expansion of Sca1-derived neointimal cells following injury [11] where the Hh pathway reportedly acts upstream of the Hippo pathway to regulate stem cell maintenance [80]. Indeed, our data suggest S100β cells are also present in normal vessels within the adventitial layer where Hh components reside [81,82]. In arteriosclerotic lesions, S100β expression is exaggerated within the neointimal layer with sparse staining for PTCH1 present. As S100β NEP-derived SMCs are considered crucial to the generation of SMC in vascular lesions within atheroprone regions of the murine vasculature [4,43], it is tempting to speculate that Hh responsive S100β-derived SMC-like progeny may also play a pivotal role in lesion formation in humans. Future studies that address the interactions between Hippo pathway and Hh may yield therapeutic strategies aimed at interfering with YAP activity through inhibition of hedgehog pathway, which downregulates the YAP protein [83,84].

In conclusion, the identification of a population of S100β/Sca1 cells within vascular lesions that are derived from a non-SMC S100β parent population is novel and highlights these cells as an important source for intimal thickening following injury. Furthermore, the role of SHh in mediating this process expands our understanding of the mechanisms contributing to the progression of vascular lesions. While Hh signalling has previously been implicated in the development of vascular lesions through modulation of a differentiated SMC phenotype [28], our study further suggests that Hh signalling may also control myogenic differentiation and accumulation S100β/Sca1 derived SMC-like progeny within vascular lesions. While hedgehog signalling appears critical, further research is required to investigate the precise mechanisms

driving migration, proliferation and differentiation of stem cells during lesion formation. It is possible that SMC-like cells within lesions comprise several different stages of the myogenic, osteogenic and myeloid differentiation of various stem cells and hence display a variety of divergent phenotypes. The elucidation of these mechanisms will provide vital information needed for the development of more efficient and novel therapies for vascular proliferative diseases. Our results provide a potential strategy for the treatment of atherosclerosis by combating cell migration and asymmetric differentiation of a perivascular-derived S100β parent vSC population.

Methods

Mice Breeding and Genotyping

All procedures were approved by the University of Rochester Animal Care Committee in accordance with the guidelines of the National Institutes of Health for the Care and Use of Laboratory Animals. Sca1-eGFP transgenic mice were obtained from JAX labs; Stock #012643, strain name B6.Cg.Tg(Ly6a-EGFP)G5Dzk/j. These transgenic mice have an enhanced green fluorescent protein (eGFP) under the control of murine lymphocyte antigen 6 complex, locus A (Ly6a) promoter. Hemizygous Ly6a-GFP mice are viable, fertile, normal in size and do not display any gross physical or behavioural abnormalities [85].

S100β-EGFP/Cre/ERT2 transgenic mice (JAX Labs, stock #014160, strain name B6;DBA-Tg(S100β-EGFP/cre/ERT2)22Amc/j) express the eGFPCreER^{T2} (Enhanced Green Fluorescent Protein and tamoxifen inducible cre recombinase/ESR1) fusion gene under the direction of the mouse S100β promoter. Ai9 mice (Jax Labs, stock #007909, strain name B6.Cg-Gt(ROSA)26Sor$^{tm9(CAG\text{-}tdTomato)Hze}$ /J) express robust tdTomato fluorescence following Cre-mediated LoxP recombination. For lineage tracing experiments S100β-eGFP/Cre/ERT2–dTomato double transgenic mice of both genders were generated by crossing S100β-eGFP/Cre-ERT2 mice with Ai9 reporter mice. The tdTomato transgene expression pattern corresponds to genomic marked S100β cells, and the eGFP transgene expression pattern corresponds to constitutive expression of S100β. Mice were genotyped using genomic DNA prepared from tail samples. All male and female mice were included in the study and were 8-10 weeks old.

Tamoxifen-induced genetic lineage tracing

S100β-CreER-Rosa26tdT mice (average weight 20g, 6-8 wks old) were injected IP with tamoxifen (Tm) dissolved in corn oil at 75 mg/kg for 5 consecutive days. Carotid artery ligation (partial, or complete), or sham operation, was performed at 1 wk or 4 wks after the last injection of Tm. At the indicated time post-ligation or sham operation, anesthetized mice were perfusion fixed and carotid arteries harvested for analysis.

512 **Carotid Artery Ligation**

513 Ligation of the left common carotid artery was performed essentially as described previously
514 [38] one and four weeks after Tm-induced cre-recombination, in male and female S100β-
515 eGFP/Cre/ERT2–dTomato double transgenic mice. Prior to surgery mice received a single dose
516 of Buprenorphine SR (sustained release) analgesia (0.5-1.0 mg/kg SQ) (and every 72 hrs
517 thereafter as needed). The animal was clipped and the surgical site prepped using betadine
518 solution and alcohol. A midline cervical incision was made. For partial carotid artery ligation,
519 with the aid of a dissecting microscope, the left external and internal carotid arterial branches
520 were isolated and ligated with 6-0 silk suture reducing left carotid blood flow to flow via the
521 patent occipital artery. The neck incision (2 layers, muscle and skin) was sutured closed.
522 Partial ligation of the left carotid artery in this manner resulted in a decrease (~80%) in blood
523 flow, leaving an intact endothelial monolayer. Buprenorphine was administered at least once
524 post-op 6-12 hrs. For complete ligation, the left common carotid was isolated and ligated just
525 beneath the bifurcation with 6-0 silk suture. In sham surgery group, carotid was similarly
526 manipulated but not ligated. The neck incision (2 layers, muscle and skin) was sutured closed
527 and the animal allowed recover under observation. After 3, 7, 14 and 21 days, mice were
528 perfused with 4% PFA via the left ventricle for 10 min, and carotid arteries were harvested for
529 analysis.

530 **Cyclopamine treatment**

531 Sca1-eGFP mice were treated with the smoothened inhibitor, cyclopamine, or the vehicle 2-
532 hydropropyl-β-cyclodextrin (HβCD) (Sigma-Aldrich) alone as a control, (essentially as
533 described previously) [86]. Mice were injected (250 µl max volume) intraperitoneally (IP) 1 day
534 before ligation, then every other day after ligation at a dose of 10 mg/kg Cyclopamine (Sigma-
535 Aldrich) dissolved in a solution of 45% (w/v) HβCD. There was no effect of cyclopamine
536 treatment on mouse body weight, compared to the HβCD vehicle control group (data not
537 shown).

538 **Histomorphometry**

539 At specified times post-ligation, mice were anesthetized (ketamine/xylazine) and perfusion
540 fixed with 4% paraformaldehyde in sodium phosphate buffer (pH 7.0). Fixed carotids were
541 embedded in paraffin for sectioning. Starting at the carotid bifurcation landmark (single

542 lumen) a series of cross-sections (10 x 5 µm) were made, every 200 µm through 2 mm length
543 of carotid artery. Cross-sections were de-paraffinized, rehydrated in graded alcohols and
544 stained with Verhoeff-Van Gieson stain for elastic laminae and imaged using a Nikon TE300
545 microscope equipped with a Spot RT digital camera (Diagnostic Instruments). Digitized images
546 were analyzed using SPOT Advanced imaging software. Assuming a circular structure *in vivo*,
547 the circumference of the lumen was used to calculate the lumen area, the intimal area was
548 defined by the luminal surface and internal elastic lamina (IEL), the medial area was defined
549 by the IEL and external elastic lamina (EEL), and the adventitial area was the area between
550 the EEL and the outer edge, essentially as described by us previously [38]

551 **Haematoxylin and Eosin Staining of Tissue**

552 For human artery cross sections, slides were placed in ice-cold acetone and held at -20°C for
553 15 min. They were then washed 3 x PBS before immersion in Harris Haematoxylin at room
554 temperature for 8 min. Slides were processed by sequential washing – in distilled water for 5
555 min; 1 % acid alcohol for 30 sec; 0.1 % sodium bicarbonate for 1 min and 95 % ethanol. Slides
556 were then washed in Eosin for 1 min, 75 % ethanol for 3 min, 95 % ethanol for 3 min and 100
557 % ethanol for 3 min before being submerged in Histoclear for 3 min and permanently
558 mounted using 3 drops of DPX, cleaned with 100 % ethanol before analysis.

559 For murine vessels, paraffin rehydration was conducted at room temperature by immersing
560 the slides in xylene for 20 minutes. The slides were then immersed in the following gradients
561 of ethanol for 5 minutes respectively: 100 %, 90 %, 70 % and 50 % ethanol. The slides were
562 then rinsed in distilled H_2O_2 before washing in 1x PBS for 10 minutes. The slides were stored
563 in 1x PBS until ready when they were immersed in Harris Haematoxylin at room temperature
564 for 8 min.

565 S100β$^+$ cells were identified as either "genomically marked" red tdTomato expressing cells or
566 "currently expressing" green fluorescent protein (eGFP) cells visualized in deparaffinized
567 S100β-eGFP/Cre/ERT2–dTomato mouse carotid cross sections mounted with Sigma
568 Fluoroshield with DAPI, using an FV1000 Olympus or a Nikon A1R HD laser scanning confocal
569 microscope. Numbers of red or green fluorescent cells and DAPI nuclei (blue) in carotid cross
570 section images from different experimental groups were either analyzed by Fiji ImageJ
571 software in each vessel compartment using a grid system.

572 **Whole mount histochemical analysis**

573 Briefly, arteries harvested from transgenic mice were washed in PBS before transfer to 10 %
574 neutral buffered formalin and incubated at 4 °C overnight. The tissue was rinsed 3 x PBS
575 before mounting on histology slides using DAPI containing fluoroshield (Sigma). The whole
576 tissue was then imaged using a Nikon Eclipse TS100 inverted microscope, EXFO X-Cite™ 120
577 fluorescence system and assessed using SPOT imaging software.

578 **Immunofluorescent Staining of tissues.**

579 Immunostaining essentially as previously described [38]. Carotid artery cryosections were air-
580 dried for 1 h at room temperature, followed by incubation with blocking buffer (5% donkey
581 serum, 0.1% Triton X-100 in PBS) for 30 minutes at room temperature and then incubated
582 with primary antibody overnight at 4^0C in antibody solution (2.5% BSA, 0.3M Glycine and 1%
583 Tween in DPBS). Murine and human arterial sections were stained with primary antibodies
584 [Supplementary Table I]. Isotype IgG control and secondary antibody only controls were
585 performed. For antigen retrieval, slides were brought to a boil in 10 mM sodium citrate (pH
586 6.0) then maintained at a sub-boiling temperature for 10 minutes. Slides were cooled on the
587 bench-top for 30 minutes then washed in deionized water (3 x 5 min) each before being
588 washed in PBS (3 x 5 min). The antigen retrieval protocol diminishes endogenous eGFP and
589 tdT tomato transgene signals. Therefore, those sections were co-stained with anti-eGFP
590 antibody and anti-Td tomato antibody [Supplementary Table I].

591 For immunofluorescence staining, 5 consecutive images were obtained and processed using
592 ImageJ software™ to analyze the collected images. Mouse carotid artery cross sections were
593 mounted with fluoroshield with DAPI and analyzed using an FV1000 Olympus or a Nikon A1R
594 HD laser scanning confocal microscope. Images were merged using the Image color-merge
595 channels function. Merged signals and split channels were used to delineate the signals at
596 single-cell resolution. Settings were fixed at the beginning of both acquisition and analysis
597 steps and were unchanged. Brightness and contrast were lightly adjusted after merging.

598 **Immunocytofluorescent staining of cells**

599 Cells seeded onto UV sterilized coverslips were fixed with 3.7 % formaldehyde, (15 min, RT). If
600 cells required permeabilization for the detection of intracellular antigens, cells were

601 incubated in 0.025 % Triton X-100 PBS (room temp, 15 min). All coverslips were blocked (1 hr,
602 RT) using 5 % BSA, 0.3 M Glycine, 1 % Tween PBS solution (1 hr, RT). Cells were incubated
603 with primary antibodies overnight at 4°C [Supplemental Table II], then washed twice with PBS
604 to remove any unbound primary antibody before being incubated (1 hr, RT) with the
605 recommended concentration of fluorochrome-conjugated secondary antibodies diluted in
606 blocking buffer [Supplementary Table II]. Following 2x wash in PBS, cell nuclei were stained
607 using DAPI: PBS (dilution 1:1000) (15 min, RT). For each primary and secondary antibody
608 used, a secondary control and an IgG isotype control was performed to assess nonspecific
609 binding. An Olympus CK30 microscope and FCell™ software was used to capture images.
610 Images were analyzed using ImageJ software as described above. Settings were fixed at the
611 beginning of both acquisition and analysis steps and were unchanged. Brightness and contrast
612 were lightly adjusted after merging.

613 **Cell culture and harvesting**

614 Murine aortic SMCs (MOVAS (ATCC® CRL-2797™) were cultured in Dulbeco's Modified Eagles
615 growth medium (DMEM) supplemented with Fetal Bovine Serum (10%), L-glutamine (2 mM,
616 Gibco) and Penicillin-Streptomycin (100U/mL, Gibco). Murine neuroectodermal stem cells
617 (mNE-4Cs, ATCC® CRL-2925™) were grown in Eagle's Minimum Essential Medium
618 supplemented with Fetal Bovine Serum (10%), L-glutamine (2 mM, Gibco) and Penicillin-
619 Streptomycin (100U/mL, Gibco) using Poly-L-Lysine coated plates (15 µg/ml). Murine
620 embryonic C3H 10T1/2 cells (ATCC® CRL-226™) were grown in Eagle's Basal medium
621 supplemented with heat-inactivated fetal bovine serum to a final concentration of 10% and
622 2mM L-glutamine. Murine embryonic stem cells (mESCs) ES-D3 [D3] (ATCC® CRL-1934™) were
623 maintained in culture in Mouse ES Cell Basal Medium (ATCC SCRR-2011) supplemented with
624 2-mercaptoethanol (0.1 mM) and 15% ES-Cell Qualified FBS (ATCC SCRR-30-2020) and a 1,000
625 U/mL mouse leukemia inhibitory factor (LIF) (Millipore Cat. No. ESG1107). Murine vSCs from
626 AA and TA regions of the mouse aorta were grown in DMEM media supplemented with chick
627 embryo extract (2%), FBS embryonic qualified (1%, ATCC), B-27 Supplement, serum free, N-2
628 Supplement (Cell Therapy Systems), recombinant mouse bFGF (0.02 µg/mL), 2-
629 Mercaptoethanol (50nM), retinoic acid (100 nM), Penicillin-Streptomycin (100U/mL, Gibco)
630 (MM).

631 **Isolation of S100β/Sca1 murine resident vascular stem cells (vSCs)**

632 Using an optimised enzymatic cell dissociation technique protocol vSCs from both
633 atheroprone (aortic arch - neuroectodermal, NE), and athero-resistant (thoracic aorta-
634 paraxial mesodermal, PM) regions of the murine aorta were isolated using sequential seeding
635 on adherent and non—adherent plates. Mouse thoracic aortas (4 at a time) were harvested
636 and placed in cold Hank's solution for adipose tissue removal and lumen rinsing. The
637 adventitia was enzymatically removed by incubation of the vessels in collagenase solution of
638 MEMα containing GlutaMAX™ (2 ml), collagenase type 1A (0.7 mg/ml), soybean trypsin
639 inhibitor (50 mg/ml), and bovine serum albumin (1 mg/ml) for approx. 10-20 min at 37°C.
640 Once the adventitia became lose, it was carefully removed as an intact layer using forceps
641 under a dissecting microscope. The aorta was divided into aortic arch (AA) and thoracic aorta
642 (TA) regions and cut into 1 mm pieces and digested with Elastase type III (Sigma) at 37°C.
643 Dispersed cells were centrifuged and washed twice in warm maintenance medium (MM)
644 (DMEM supplemented with 2% chick embryo extract, 1% FBS, 0.02 µg/ml, bFGF basic protein,
645 B-27 Supplement, N-2 supplement, 1% Penicillin-Streptomycin, 50 nM 2-Mercaptoethanol
646 and 100 nM retinoic acid) before seeding (1st seeding) on a 6-well non-adherent plate in MM.
647 At 48 h, suspension cells were transferred (2nd seeding) to a fresh well of a CELLstart™ pre-
648 coated 6-well plate in MM. Additional MM was added to the remaining cells in the non-
649 adherent surface. Cells were incubated at 37°C, 5% CO_2 for 1 week with minimal disturbance.
650 The stem cells exhibited a uniform neural-like morphology in low density culture adopting a
651 dendritic-like tree shape and retaining their morphological characteristics at low density
652 throughout repeated passage. Cells were fed with MM every 2-3 days and passaged every 3-4
653 days or when ~70% confluent.

654 **Generation of human neuroectoderm progenitors (NEPs) from induced pluripotent stem**
655 **cells (HiPSCs)**

656 Human induced pluripotent stem cells (HiPSC) were obtained from HipSci (Cambridge, UK)
657 and cultured per the manufacturer's instructions. Briefly, human dermal fibroblasts were
658 isolated from excess skin of patients undergoing plastic surgery and reprogrammed as
659 previously described [87]. HiPSCs were grown on plates pre-coated using Vitronectin (10 µg/ml)
660 and maintained in complete Essential eight medium replacing 95% of the medium daily. A
661 ROCK inhibitor (10 µM) was added to optimize colony growth. Cells were sub-cultured with
662 0.05 mM EDTA for 4-8 min at room temperature until colonies displayed bright halos around

663 the edges and small holes appeared throughout. Cells were frozen down in knock-out serum
664 solution with 10% DMSO. HiPSCs at 70% confluency were routinely split at a ratio of 1:10 and
665 cells were used between passage 20-40.

666 For neuroectoderm differentiation, cells were grown in chemically defined neuroectodermal
667 medium (CDM) containing IMDM, F12 nutrient mix, chemically defined lipid concentrate,
668 transferrin, monothioglycerol, penicillin-streptomycin and 0.5 g of PVA, and insulin, as
669 previously described [43]. Neuroectoderm differentiation was initiated in CDM supplemented
670 with FGF2 (12 ng/ml) and SB431542 (10 µM) for 7 days. Neuroectodermal (NE) progenitors
671 were maintained in CDM-PVA supplemented with FGF2 (12 ng/ml) and SB431542 (10 µM) and
672 sub-cultured using TrypLE™ for 3–5 min at 37°C in a 5% CO_2 incubator. NE progenitors were
673 used between passage 1-10.

674 To initiate myogenic SMC differentiation, NEPs were subcultured in SMC differentiation
675 medium containing CDM + PDGF-BB (10 ng/ml, PeproTech) + TGF-β1 (2 ng/ml, PeproTech) for
676 12 days. Neuroectoderm-derived SMCs (NE-SMC) were maintained in CDM supplemented
677 with 10% FBS. After 12 d of PDGF-BB and TGF-β1 treatment, all cells appeared spindle-
678 shaped. Complete medium was then changed to DMEM 10% FBS, 1% Penicillin streptomycin
679 for expansion. Cells were frozen down using 90% (volume/volume) FBS + 10% (vol/vol) DMSO.
680 The NE-SMC were used between passage 3-20.

681 **Human tissue**

682 Tissue sections from paired normal human aorta and arteriosclerotic vessels were obtained
683 from Amsbio LLC, tissue repository.

684 **Chromatin Immunoprecipitation**

685 ChIP was performed on cultured cells as previously described with slight modifications [79].
686 Cells at 70% confluency were fixed with 1% paraformaldehyde (10 min, RT). Cross-link was
687 stopped by addition of 125 mM glycine for 10 min. The cross-linked chromatin was sonicated
688 to shear chromatin into fragments of 200–600 base pairs. The sheared chromatin was
689 immunoprecipitated with 2 µg tri-methyl-histone H3 (Lys27) and di-methyl-histone H3 (Lys4),
690 while negative control was incubated with mouse IgG and input DNA without antibody using
691 the CHIP—IT Express HT Kit from Active Motif (Cat no: 53018) according to the

692 manufacturer's instructions [Supplementary Table III]. A chromatin IP DNA Purification Kit
693 (Cat No 58002 Active Motif) was used to purify the samples after CHIP before PCR was
694 performed using Myh11 primers [5' -CCC TCC CTT TGC TAA ACA CA - 3' and 5' - CCA GAT CCT
695 GGG TCC TTA CA – 3]. Sensimix SYBR® no-ROX Bioline Kit (QT650) was used to perform Real
696 Time One-Step PCR according to the manufacturers' instructions. The antibodies used for
697 ChIP are outlined in Supplemental Table I

698 **Quantitative PCR**

699 Total RNA was prepared from cultured cells using the ReliaPrep™ RNA Cell Miniprep System
700 kit from Promega according to the manufacturer's protocol. Two micrograms of RNA was
701 used for reverse transcription with Rotor-Gene SYBR Green RT-PCR (QIAGEN) or The
702 SensiMix™ SYBR® No-ROX (BioLine) protocols for Real TimeOne-Step RT-PCR using the Real
703 Time Rotor-GeneRG-3000™ light cycler from Corbett Research using primers listed in
704 Supplementary Table IV.

705 **Flow cytometry and analysis**

706 Isolated cells were incubated with I fluorochrome-conjugated antibodies and control IgG's or
707 (ii) the appropriate primary antibody with fluorochrome-conjugated secondary antibodies at a
708 final concentration of 1µg per sample and incubated at 4°C for 30 minutes [Supplementary
709 Table V]. Fluorescence labeled cells analysis was performed using a BD FACS Aria flow
710 cytometry system (BD Biosciences), and data were analyzed with FlowJo™ software (Tree
711 Star, Ashland, Ore) and De Novo software FCS Express 4 Flow Cytometry (Pasadena, CA)

712 **Telomere Assay**

713 The average telomere length in cells was measured using a ScienCell's Absolute Mouse
714 Telomere Length Quantification qPCR Assay Kit (AMTLQ) according to the manufacturer's
715 instructions. The telomere primer set recognizes and amplifies telomere sequences and is
716 designed to directly measure the average telomere length of murine cells.

717 **QUANTIFICATION AND STATISTICAL ANALYSIS**

718 All data were determined from multiple individual biological samples and presented as mean
719 values ± standard error of the mean (SEM). All in vitro experiments were performed in

triplicate and repeated three times unless otherwise stated. All mice were randomly assigned to groups (including both male and female), and the analysis was performed blind by two groups. For statistical comparisons, all data was checked for normal gaussian distribution before parametric and non-parametric tests were performed. An unpaired two-sided Student's t-test was performed using GraphPad Prism software v9™ for comparing differences between two groups, and ANOVA test for over multiple comparisons. Significance was accepted when $p \leq 0.05$.

Data Availability:

The data, materials and reagents generated or analysed that support the findings of this study are available from the corresponding authors (PAC and EMR) on reasonable request.

Acknowledgments:

We thank Diana Scott for histological tissue processing, and Drs. Linda Callahan and Paivi Jordan for confocal microscope expertise. This research was funded in part by Science Foundation Ireland grant SFI-11/PI/1128, Health Research Board (HRB) of Ireland grant HRA-POR-2015-1315, the European Union's INTERREG VA Programme, managed by the Special EU Programmes Body (SEUPB) to PAC, and NIH R21AA020365 and R21AA023213 to EMR, Irish Research Council (IRC) GOIPG/2014/43 (M.DiL) and GOIPG/2016/1529 (E.C), King Abdulla Scholarship IR15208 ID1066336148 to Y.G.

Author Contributions:

E.F., W.L., J-C.H, performed the animal experiments and M.DiL and SH performed the blind analysis of the images. E.F performed the human arteriosclerotic tissue analysis. E.F., M.DiL., R.H., D.B., E.C., performed the murine and rat cell culture experiments, D.B performed the HiPSCs cell work. EC performed the telomere assay and R.H.J, MdiL and Y.G., performed the ChIP analysis. E.M.R., C.L., and P.A.C drafted the manuscript, revised the manuscript and discussed the results. E.M.R., and P.A.C., designed and coordinated the experiments, interpreted the data, revised and confirmed the paper. All authors reviewed and confirmed the manuscript.

Competing Interests:

The authors declare no financial and non-financial conflicts of interest.

754 **References**

755 1. Bennett, M. R., Sinha, S. & Owens, G. K. Vascular Smooth Muscle Cells in
756 Atherosclerosis. *Circ. Res.* **118**, 692–702 (2016).
757 2. Sakamoto, A. *et al.* Pathologic intimal thickening: Are we any closer to understand early
758 transitional plaques that lead to symptomatic disease? *Atherosclerosis* **274**, 227–229
759 (2018).
760 3. Halcox, J. P. J. *et al.* Endothelial Function Predicts Progression of Carotid Intima-Media
761 Thickness. *Circulation* **119**, 1005–1012 (2009).
762 4. Sinha, S., Iyer, D. & Granata, A. Embryonic origins of human vascular smooth muscle
763 cells: implications for in vitro modeling and clinical application. *Cell. Mol. Life Sci.* **71**,
764 2271–88 (2014).
765 5. Korshunov, V. A. & Berk, B. C. Flow-induced vascular remodeling in the mouse: a model
766 for carotid intima-media thickening. *Arterioscler. Thromb. Vasc. Biol.* **23**, 2185–91
767 (2003).
768 6. Liu, W., Redmond, E. M., Morrow, D. & Cullen, J. P. Differential effects of daily-
769 moderate versus weekend-binge alcohol consumption on atherosclerotic plaque
770 development in mice. *Atherosclerosis* **219**, 448–54 (2011).
771 7. Nam, D. *et al.* Partial carotid ligation is a model of acutely induced disturbed flow,
772 leading to rapid endothelial dysfunction and atherosclerosis. *Am. J. Physiol. Heart Circ.*
773 *Physiol.* **297**, H1535-43 (2009).
774 8. Chappell, J. *et al.* Extensive Proliferation of a Subset of Differentiated, yet Plastic,
775 Medial Vascular Smooth Muscle Cells Contributes to Neointimal Formation in Mouse
776 Injury and Atherosclerosis Models. *Circ. Res.* **119**, 1313–1323 (2016).
777 9. Dobnikar, L. *et al.* Disease-relevant transcriptional signatures identified in individual
778 smooth muscle cells from healthy mouse vessels. *Nat. Commun.* **9**, 4567 (2018).
779 10. Yuan, F. *et al.* Contribution of Vascular Cells to Neointimal Formation. *PLoS One* **12**,
780 e0168914 (2017).
781 11. Tang, J. *et al.* Arterial Sca1+ Vascular Stem Cells Generate De Novo Smooth Muscle for
782 Artery Repair and Regeneration. *Cell Stem Cell* **26**, 81-96.e4 (2020).
783 12. Tang, Z. *et al.* Differentiation of multipotent vascular stem cells contributes to vascular
784 diseases. *Nat. Commun.* **3**, 875 (2012).
785 13. Kramann, R. *et al.* Adventitial MSC-like Cells Are Progenitors of Vascular Smooth
786 Muscle Cells and Drive Vascular Calcification in Chronic Kidney Disease. *Cell Stem Cell*
787 **19**, 628–642 (2016).
788 14. Majesky, M. W. *et al.* Differentiated Smooth Muscle Cells Generate a Subpopulation of
789 Resident Vascular Progenitor Cells in the Adventitia Regulated by Klf4. *Circ. Res.* **120**,
790 296–311 (2017).
791 15. Wan, M. *et al.* Injury-activated transforming growth factor β controls mobilization of
792 mesenchymal stem cells for tissue remodeling. *Stem Cells* **30**, 2498–511 (2012).
793 16. Donato, R. *et al.* S100B's double life: intracellular regulator and extracellular signal.
794 *Biochim. Biophys. Acta* **1793**, 1008–22 (2009).
795 17. Cao, T. *et al.* S100B promotes injury-induced vascular remodeling through modulating
796 smooth muscle phenotype. *Biochim. Biophys. Acta - Mol. Basis Dis.* **1863**, 2772–2782
797 (2017).
798 18. Sagheddu, R. *et al.* Targeting RAGE as a potential therapeutic approach to Duchenne
799 muscular dystrophy. *Hum. Mol. Genet.* **27**, 3734–3746 (2018).
800 19. Zhou, S., Zhu, W., Zhang, Y., Pan, S. & Bao, J. S100B promotes microglia M1 polarization
801 and migration to aggravate cerebral ischemia. *Inflamm. Res.* **67**, 937–949 (2018).

20. Wu, Y. *et al.* S100B is required for maintaining an intermediate state with double-positive Sca-1+ progenitor and vascular smooth muscle cells during neointimal formation. *Stem Cell Res. Ther.* **10**, 294 (2019).
21. Petrova, R. & Joyner, A. L. Roles for Hedgehog signaling in adult organ homeostasis and repair. *Development (Cambridge)* vol. 141 3445–3457 (2014).
22. Marigo, V., Davey, R. A., Zuo, Y., Cunningham, J. M. & Tabin, C. J. Biochemical evidence that patched is the hedgehog receptor. *Nature* **384**, 176–179 (1996).
23. Briscoe, J. & Thérond, P. P. The mechanisms of Hedgehog signalling and its roles in development and disease. *Nat. Rev. Mol. Cell Biol.* **14**, 416–429 (2013).
24. Marigo, V. & Tabin, C. J. Regulation of patched by Sonic hedgehog in the developing neural tube. *Proc. Natl. Acad. Sci. U. S. A.* **93**, 9346–9351 (1996).
25. Marigo, V., Johnson, R. L., Vortkamp, A. & Tabin, C. J. Sonic hedgehog differentially regulates expression of GLI and GLI3 during limb development. *Dev. Biol.* **180**, 273–283 (1996).
26. Chuang, P. T. & McMahon, A. P. Vertebrate hedgehog signalling modulated by induction of a hedgehog- binding protein. *Nature* **397**, 617–621 (1999).
27. Schunkert, H. *et al.* Large-scale association analysis identifies 13 new susceptibility loci for coronary artery disease. *Nat. Genet.* **43**, 333–8 (2011).
28. Aravani, D. *et al. HHIPL1* , a Gene at the 14q32 Coronary Artery Disease Locus, Positively Regulates Hedgehog Signaling and Promotes Atherosclerosis. *Circulation* **140**, 500–513 (2019).
29. Beckers, L. *et al.* Disruption of hedgehog signalling in ApoE - /- mice reduces plasma lipid levels, but increases atherosclerosis due to enhanced lipid uptake by macrophages. *J. Pathol.* **212**, 420–8 (2007).
30. Ali, H. *et al.* Localization and characterization of a novel secreted protein, SCUBE2, in the development and progression of atherosclerosis. *Kobe J. Med. Sci.* **59**, E122-31 (2013).
31. Dutzmann, J. *et al.* Sonic hedgehog-dependent activation of adventitial fibroblasts promotes neointima formation. *Cardiovasc. Res.* **113**, 1653–1663 (2017).
32. Morrow, D. *et al.* Sonic Hedgehog induces Notch target gene expression in vascular smooth muscle cells via VEGF-A. *Arterioscler. Thromb. Vasc. Biol.* **29**, 1112–8 (2009).
33. Li, F. *et al.* Sonic hedgehog signaling induces vascular smooth muscle cell proliferation via induction of the G1 cyclin-retinoblastoma axis. *Arterioscler. Thromb. Vasc. Biol.* **30**, 1787–94 (2010).
34. Wang, G. *et al.* Activation of the sonic hedgehog signaling controls human pulmonary arterial smooth muscle cell proliferation in response to hypoxia. *Biochim. Biophys. Acta* **1803**, 1359–67 (2010).
35. Passman, J. N. *et al.* A sonic hedgehog signaling domain in the arterial adventitia supports resident Sca1+ smooth muscle progenitor cells. *Proc. Natl. Acad. Sci. U. S. A.* **105**, 9349–54 (2008).
36. Shikatani, E. A. *et al.* c-Myb Regulates Proliferation and Differentiation of Adventitial Sca1+ Vascular Smooth Muscle Cell Progenitors by Transactivation of Myocardin. *Arterioscler. Thromb. Vasc. Biol.* **36**, 1367–76 (2016).
37. Tsai, T.-N. *et al.* Contribution of stem cells to neointimal formation of decellularized vessel grafts in a novel mouse model. *Am. J. Pathol.* **181**, 362–73 (2012).
38. Fitzpatrick, E. *et al.* Alcohol Reduces Arterial Remodeling by Inhibiting Sonic Hedgehog-Stimulated Stem Cell Antigen-1 Positive Progenitor Stem Cell Expansion. *Alcohol. Clin. Exp. Res.* **41**, 2051–2065 (2017).

39. Redmond, E. M. *et al.* Inhibition of patched-1 prevents injury-induced neointimal hyperplasia. *Arterioscler. Thromb. Vasc. Biol.* **33**, 1960–4 (2013).
40. Fang, Y., Wu, D. & Birukov, K. G. Mechanosensing and mechanoregulation of endothelial cell functions. *Compr. Physiol.* **9**, 873–904 (2019).
41. Reinert, R. B. *et al.* Tamoxifen-Induced Cre-loxP Recombination Is Prolonged in Pancreatic Islets of Adult Mice. *PLoS One* **7**, e33529 (2012).
42. Kennedy, E. *et al.* Embryonic rat vascular smooth muscle cells revisited - a model for neonatal, neointimal SMC or differentiated vascular stem cells? *Vasc. Cell* **6**, 6 (2014).
43. Cheung, C., Bernardo, A. S., Trotter, M. W. B., Pedersen, R. A. & Sinha, S. Generation of human vascular smooth muscle subtypes provides insight into embryological origin-dependent disease susceptibility. *Nat. Biotechnol.* **30**, 165–73 (2012).
44. Murry, C. E., Gipaya, C. T., Bartosek, T., Benditt, E. P. & Schwartz, S. M. Monoclonality of smooth muscle cells in human atherosclerosis. *Am. J. Pathol.* **151**, 697–705 (1997).
45. Basatemur, G. L., Jørgensen, H. F., Clarke, M. C. H., Bennett, M. R. & Mallat, Z. Vascular smooth muscle cells in atherosclerosis. *Nat. Rev. Cardiol.* **16**, 727–744 (2019).
46. Gomez, D. & Owens, G. K. Reconciling Smooth Muscle Cell Oligoclonality and Proliferative Capacity in Experimental Atherosclerosis. *Circ. Res.* **119**, 1262–1264 (2016).
47. Hoglund, V. J., Dong, X. R. & Majesky, M. W. Neointima formation: a local affair. *Arterioscler. Thromb. Vasc. Biol.* **30**, 1877–9 (2010).
48. Nguyen, A. T. *et al.* Smooth muscle cell plasticity: fact or fiction? *Circ. Res.* **112**, 17–22 (2013).
49. Campbell, J. H. & Campbell, G. R. Smooth Muscle Phenotypic Modulation—A Personal Experience. *Arterioscler. Thromb. Vasc. Biol.* **32**, 1784–1789 (2012).
50. Cooley, B. C. *et al.* TGF- Signaling Mediates Endothelial-to-Mesenchymal Transition (EndMT) During Vein Graft Remodeling. *Sci. Transl. Med.* **6**, 227ra34-227ra34 (2014).
51. Nemenoff, R. A. *et al.* SDF-1α induction in mature smooth muscle cells by inactivation of PTEN is a critical mediator of exacerbated injury-induced neointima formation. *Arterioscler. Thromb. Vasc. Biol.* **31**, 1300–8 (2011).
52. Herring, B., Hoggatt, A. M., Burlak, C. & Offermanns, S. Previously differentiated medial vascular smooth muscle cells contribute to neointima formation following vascular injury. *Vasc. Cell* **6**, 21 (2014).
53. Shankman, L. S. *et al.* KLF4-dependent phenotypic modulation of smooth muscle cells has a key role in atherosclerotic plaque pathogenesis. *Nat. Med.* **21**, 628–637 (2015).
54. Owens, G. K. Molecular control of vascular smooth muscle cell differentiation and phenotypic plasticity. *Novartis Found. Symp.* **283**, 174–91; discussion 191-3, 238–41 (2007).
55. Chakraborty, R. *et al.* Promoters to Study Vascular Smooth Muscle. *Arterioscler. Thromb. Vasc. Biol.* **39**, 603–612 (2019).
56. Murgai, M. *et al.* KLF4-dependent perivascular cell plasticity mediates pre-metastatic niche formation and metastasis. *Nat. Med.* **23**, 1176–1190 (2017).
57. Sheikh, A. Q., Lighthouse, J. K. & Greif, D. M. Recapitulation of Developing Artery Muscularization in Pulmonary Hypertension. *Cell Rep.* **6**, 809–817 (2014).
58. Roostalu, U. *et al.* Distinct Cellular Mechanisms Underlie Smooth Muscle Turnover in Vascular Development and Repair. *Circ. Res.* **122**, 267–281 (2018).
59. Tobin, S. W. *et al.* Dual roles for bone marrow–derived Sca-1 cells in cardiac function. *FASEB J.* **31**, 2905–2915 (2017).
60. Tang, Z., Wang, A., Wang, D. & Li, S. Smooth muscle cells: to be or not to be? Response

to Nguyen et Al. *Circ. Res.* **112**, 23–6 (2013).
61. Kalluri, A. S. *et al.* Single-Cell Analysis of the Normal Mouse Aorta Reveals Functionally Distinct Endothelial Cell Populations. *Circulation* **140**, 147–163 (2019).
62. Psaltis, P. J. *et al.* Characterization of a resident population of adventitial macrophage progenitor cells in postnatal vasculature. *Circ. Res.* **115**, 364–375 (2014).
63. Hu, Y. *et al.* Abundant progenitor cells in the adventitia contribute to atherosclerosis of vein grafts in ApoE-deficient mice. *J. Clin. Invest.* **113**, 1258–65 (2004).
64. Wang, Y.-L., Liu, L.-Z., He, Z.-H., Ding, K.-H. & Xue, F. Phenotypic transformation and migration of adventitial cells following angioplasty. *Exp. Ther. Med.* **4**, 26–32 (2012).
65. Campbell, G. J. & Roach, M. R. Fenestrations in the internal elastic lamina at bifurcations of human cerebral arteries. *Stroke* **12**, 489–96.
66. Wong, L. C. Y. & Langille, B. L. Developmental Remodeling of the Internal Elastic Lamina of Rabbit Arteries. *Circ. Res.* **78**, 799–805 (1996).
67. Guo, Z.-Y., Yan, Z.-Q., Bai, L., Zhang, M.-L. & Jiang, Z.-L. Flow shear stress affects macromolecular accumulation through modulation of internal elastic lamina fenestrae. *Clin. Biomech.* **23**, S104–S111 (2008).
68. Chen, Q. *et al.* Genetic lineage tracing analysis of c-kit+ stem/progenitor cells revealed a contribution to vascular injury-induced neointimal lesions. *J. Mol. Cell. Cardiol.* **121**, 277–286 (2018).
69. Skelly, C. L., Chandiwal, A., Vosicky, J. E., Weichselbaum, R. R. & Roizman, B. Attenuated herpes simplex virus 1 blocks arterial apoptosis and intimal hyperplasia induced by balloon angioplasty and reduced blood flow. *Proc. Natl. Acad. Sci. U. S. A.* **104**, 12474–12478 (2007).
70. Moonen, J.-R. A. J. *et al.* Endothelial-to-mesenchymal transition contributes to fibro-proliferative vascular disease and is modulated by fluid shear stress. *Cardiovasc. Res.* **108**, 377–86 (2015).
71. Souilhol, C., Harmsen, M. C., Evans, P. C. & Krenning, G. Endothelial–mesenchymal transition in atherosclerosis. *Cardiovasc. Res.* **114**, 565–577 (2018).
72. Pan, L. *et al.* Shear stress induces human aortic endothelial cell apoptosis via interleukin-1 receptor-associated kinase 2-induced endoplasmic reticulum stress. *Mol. Med. Rep.* **16**, 7205–7212 (2017).
73. Heo, K.-S. *et al.* PKCζ mediates disturbed flow-induced endothelial apoptosis via p53 SUMOylation. *J. Cell Biol.* **193**, 867–884 (2011).
74. Dong, G. *et al.* Low shear stress-induced autophagy alleviates cell apoptosis in HUVECs. *Mol. Med. Rep.* **15**, 3076–3082 (2017).
75. Zhang, Y. *et al.* Protective effect of irisin on atherosclerosis via suppressing oxidized low density lipoprotein induced vascular inflammation and endothelial dysfunction. *PLoS One* **11**, (2016).
76. Franck, G. *et al.* Flow Perturbation Mediates Neutrophil Recruitment and Potentiates Endothelial Injury via TLR2 in Mice: Implications for Superficial Erosion. *Circ. Res.* **121**, 31–42 (2017).
77. Bentzon, J. F. & Majesky, M. W. Lineage tracking of origin and fate of smooth muscle cells in atherosclerosis. *Cardiovasc. Res.* **114**, 492–500 (2018).
78. van der Harst, P. & Verweij, N. Identification of 64 Novel Genetic Loci Provides an Expanded View on the Genetic Architecture of Coronary Artery Disease. *Circ. Res.* **122**, 433–443 (2018).
79. Gomez, D., Shankman, L. S., Nguyen, A. T. & Owens, G. K. Detection of histone modifications at specific gene loci in single cells in histological sections. *Nat. Methods*

10, 171–177 (2013).
80. Fernandez-L, A. *et al.* YAP1 is amplified and up-regulated in hedgehog-associated medulloblastomas and mediates Sonic hedgehog-driven neural precursor proliferation. *Genes Dev.* **23**, 2729–41 (2009).
81. Queiroz, K. C. S. *et al.* Dichotomy in Hedgehog signaling between human healthy vessel and atherosclerotic plaques. *Mol. Med.* **18**, 1122–7 (2012).
82. Dunaeva, M., van Oosterhoud, C. & Waltenberger, J. Expression of Hedgehog signaling molecules in human atherosclerotic lesions: An autopsy study. *Int. J. Cardiol.* **201**, 462–464 (2015).
83. Felley-Bosco, E. & Stahel, R. Hippo/YAP pathway for targeted therapy. *Transl. lung cancer Res.* **3**, 75–83 (2014).
84. Cotton, J. L. *et al.* YAP/TAZ and Hedgehog Coordinate Growth and Patterning in Gastrointestinal Mesenchyme. *Dev. Cell* **43**, 35-47.e4 (2017).
85. Ma, X., Robin, C., Ottersbach, K. & Dzierzak, E. The Ly6A Sca1 GFP Transgene is Expressed in all Adult Mouse Hematopoietic Stem Cells. *Stem Cells* **20**, 514–521 (2002).
86. Van Den Brink, G. R. *et al.* Sonic hedgehog regulates gastric gland morphogenesis in man and mouse. *Gastroenterology* **121**, 317–328 (2001).
87. Vallier, L. *et al.* Signaling Pathways Controlling Pluripotency and Early Cell Fate Decisions of Human Induced Pluripotent Stem Cells. *Stem Cells* **27**, 2655–2666 (2009).

Figure Legends:

Figure 1. Expression of Sca1-eGFP and S100β-eGFP cells following iatrogenic flow restriction after 3 days.

a. Morphometric analysis of adventitial, medial, intimal and luminal volumes following partial ligation of the left carotid artery compared to sham controls. Data are the mean ± SEM of 4 animals, #p<0.05 vs sham.

b-d. The number of DAPI nuclei/hpf in cross-sections of (b) adventitia, (c) media and (d) intima following partial ligation of the left carotid artery (LCA) after 3d compared to untouched (control) and sham. Data are the mean ± SEM of 3-5 representative images per animals, n=3, #p<0.05.

e. Verhoeff-Van Gieson stained sections and corresponding confocal fluorescence images of DAPI nuclei (blue), Sca1-eGFP (green) and immunofluorescence of α-actin (SMA) (red), anti-eGFP (green), anti-CD31 (red) and anti-eNOS (red) expression in ligated LCA vessels expression in sham-operated and ligated LCA vessels. Arrows highlight Sca1-eGFP expressing cells in the adventitia (A), media (M) and neointima (NI) and CD31 and eNOS in intima. Scale bar = 20µm.

f. The fraction of Sca1 cells/high power field (hpf) in the adventitia, media, and intima of sham and ligated vessels after 3 days. Data are the mean ± SEM of 3- 5 sections, #p≤ 0.05 from a minimum of 4 animals per experimental group.

g. Representative immunofluorescence images for the pro-apoptotic marker, Bax, (red) in ligated left carotid artery (LCA) vessels and contralateral right carotid artery (RCA) after 3d. IgG was used as a control.

h. The number of Bax cells/hpf in the adventitia, media, and intima of sham and ligated vessels after 3d. Arrows highlight Bax expressing cells within the adventitia (A), media (M), and neointima (NI). Data are the mean ± SEM of 3-6 sections per experimental group from 3 animals. #p≤ 0.05. Scale bar = 20µm.

Figure 2. **Expression of Sca1-eGFP and S100β-eGFP cells following iatrogenic flow restriction after 7, 14 and 21 days.**

a,b. Representative Verhoeff-Van Gieson stained sections and corresponding confocal fluorescence images of DAPI nuclei (blue) and Sca1-eGFP (green) expression in LCA after (**a**) 7 days and **(b)** 14 days. Scale bar = 20µm.

c. The number of DAPI nuclei/hpf in cross-sections of adventitia, media and intima following partial ligation of the LCA after 7 and 14 days compared to sham controls. Data are the mean ± SEM of 3-5 representative images per animal, n=4.

d. The fraction of Sca1 cells/high power field (hpf) in the adventitia, media, and intima of sham and ligated vessels after 7 days and 14 days. Data are the mean ± SEM of 10-15 sections from 4 animals per experimental group.

e. Representative confocal fluorescence images of DAPI nuclei (blue), immunofluorescence of anti-eGFP (green) expression and anti-SMA (Red) in the LCA 14 days post-ligation in Sca1-eGFP mice. Data are representative of 5 images per animal.

f. Cumulative analysis of $Sca1^+$ cells, SMA^+ cells, double stained Sca1/SMA positive cells and the percentage of $Sca1^+$ cells that were $SMA1^+$ in the adventitial, medial and intimal layer of RCA and LCA vessels after 21 days, respectively. Data are the mean ± SEM, n=15-20 sections from 5 animals.

g. Representative confocal fluorescence images of DAPI nuclei (blue), immunofluorescence of anti-eGFP (green) expression and anti-Sca1 (far-red white) in sham and ligated LCA after 21 days in S100β-eGFP mice. Scale bar = 20µm.

h. Cumulative analysis of $S100β^+$ cells, $Sca1^+$ cells, double stained Sca1/S100β positive cells and the percentage of $S100β^+$ cells that were $Sca1^+$ in the adventitial, medial and intimal layer of RCA and LCA vessels, respectively after 21 days in S100β-eGFP mice. Data are the mean ± SEM, n=15-20 sections from 5 animals/group.

i. Representative confocal fluorescence images of DAPI nuclei (blue), immunofluorescence of anti-eGFP (green) expression and anti-SMA (far red, white) in the RCA and LCA 21 days post-

ligation in S100β-eGFP mice. Data are from a minimum of 4 animals per experimental group. Scale bar = 20µm.

j. Cumulative analysis of S100β$^+$ cells, SMA$^+$ cells, double stained S100β/SMA positive cells and the percentage of S100β$^+$ cells that were SMA$^+$ in the adventitial, medial and intimal layer of RCA and LCA vessels, respectively after 21 days in S100β-eGFP mice. Data are the mean ± SEM, n=15-20 sections from 4 animals/group.

Figure 3. Lineage tracing analysis of S100β-Cre(ERT2)-tdT marked cells following iatrogenic flow restriction for 21 days.

a-c. Verhoeff-Van Gieson stained sections and morphometric analysis of adventitial, medial, intimal and luminal volumes of the (**b)** contralateral RCA control compared to the **(c)** LCA following ligation for 21d. Data are the mean ± SEM of 10 images, #p<0.05 vs sham controls.

d-f. Representative confocal fluorescence images of DAPI nuclei (blue) and S100β-tdT (red) cells in mice treated with corn oil (control) or tamoxifen for 7 days prior to washout for 1 week in **(d)** sham and (**e, f**) ligated LCA. Data are minimum of 4 animals per experimental group. Scale bar = 20 µm. Arrows highlight S100β-tdT (red) marked cells.

g. Representative confocal fluorescence images of DAPI nuclei (blue), immunofluorescence of anti-tdT (red) and anti-Sca1 (far red, white) expression in the contralateral RCA and LCA 21 days post ligation. Scale bar = 20µm.

h-j. Cumulative analysis of the fraction of S100β-tdT$^+$ cells in the **(h)** RCA and **(i)** LCA and **(j)** Sca1/S100β double stained cells in the adventitial, medial and intimal layer of RCA and LCA vessels, respectively after 21 days in S100β-CreERT2-tdT mice.

Figure 4. Inhibition of Hh signalling attenuates intimal thickening and Sca1 cell expansion following iatrogenic flow restriction.

a. Representative immunofluorescence images of Hh receptor patched 1 (Ptch1) (red), Hh target gene Gli2 (red), Sca1-eGFP (green) expression and merged (eGFP/Gli2/DAPI) in carotid

artery cross sections from sham-operated, ligated vehicle control (HβCD), and ligated + cyclopamine (10 mg/kg, IP) treated mice after 14 days. Scale bar = top panel: 50µm, all other panels: 20µm.

b, c. Cumulative data showing the fraction of Sca1-eGFP cells within the adventitia, media and intima from sham-operated, ligated vehicle control (HβCD), and ligated + cyclopamine (Cyl) Sca1-eGFP mice after **(b)** 7 days and **(c)** 14 days. Data are the mean ± SEM of five sections per experimental group, #p≤ 0.05 vs ligated HβCD controls and are representative of a minimum of 4 animals per experimental group.

d, e. Representative H&E staining of carotid artery cross sections from sham, ligated control (HβCD vehicle), and ligated + cyclopamine (Cyl) treated animals after 7 d **(d)** and **(e)** 14 d. Scale bar = 50 µm.

f,g. Morphometric analysis of vessel compartment volumes for ligated control (HβCD), and ligated + cyclopamine (Cyl) treated animals after **(f)** 7d and **(g)** 14 d. Data mean ± SEM of 7-12 sections analysed from 4 animals, #p≤ 0.05 vs ligated control (HβCD).

Figure 5. Resident S100β/Sca1 vascular stem cells from atheroprone and atheroresistant regions of the mouse aorta *in vitro.*

a. Relative levels of *Myh11* and *Cnn1* in AA and TA regions of the mouse aorta. Data are expressed as the Log2 fold change in mRNA levels relative to neural stem cells (NE-4C) in culture and are the mean ± SEM of three aortic specimens, #p≤ 0.05 vs NE-4C cells. The housekeeping gene *Gapdh* was used as a control.

b, c. The level of enrichment of mRNA for neuroectodermal markers **(b)** S100β and **(c)** Sox10 within atheroprone AA (aortic arch) and atheroresistant TA (thoracic/descending aorta) regions of the mouse aorta in the absence or presence of the adventitial (Adv) layer. The housekeeping gene *hypoxanthine guanine phosphoribosyltransferase* (*hprt*) was used as a control. Data are expressed as the Log2 fold change in mRNA levels relative to murine aortic SMCs in culture and are the mean ± SEM of three aortic specimens, #p≤ 0.05 vs MOVAS SMCs.

1076 **d.** Flow cytometry analysis of vSCs isolated from AA and TA regions of the mouse aorta and
1077 grown in maintenance media for S100β (dark green) and Sca1 (light green) expression. NE-4C
1078 and CH3-10T1/2 cells were used as positive controls, respectively. Filled dark and light green
1079 curves represent negative control samples.

1080 **e,f.** Relative levels of **(e)** *Myh11* and **(f)** *Cnn1* in vSCs isolated from AA and TA regions of the
1081 mouse aorta, compared to AA and TA aortic tissue. Data are expressed as the Log2 fold
1082 change in mRNA levels relative to neural stem cells (NE-4C) in culture and are the mean ± SEM
1083 of three independent cultures and three aortic specimens, #p≤ 0.05 vs NE-4C cells.

1084 **g,h.** Representative immunocytochemical analysis of stem cell markers S100β, Nestin, Sox10,
1085 Sox17, Sca1 and SMC differentiation markers, Cnn1 and Myh11 in vSCs isolated and grown in
1086 maintenance media (MM) from **(g)** AA and **(h)** TA regions of the mouse aorta. Scale bar 20µm.

1087 **i.** Absolute telomere length of vSCs compared to cultured MOVAS SMC and fresh aortic tissue.
1088 The telomere primer set recognizes and amplifies telomere sequences. The single copy
1089 reference (SCR) primer set recognizes and amplifies a 100 bp-long region on mouse
1090 chromosome 10, and serves as reference for data normalization. Data are expressed as
1091 absolute telomere length (kb) and are the mean ± SEM of three plates and aortic specimens,
1092 #p≤ 0.05 vs MOVAs SMCs.

1093 **j,k.** Relative levels of *Gli1*, *Myh11* and *Cnn1* within vSCs isolated from **(j)** AA and **(k)** TA regions
1094 of the mouse aorta in the absence or presence of rSHh (0.5 µg/ml) with or without the
1095 smoothened inhibitor, cyclopamine (10µM). Data are expressed as the Log2 fold change in
1096 mRNA levels relative to vSCs alone (control) and are the mean ± SEM of three representative
1097 wells from two independent experiments, #p≤0.05 versus rSHh alone.

1098 **l-m.** ChiP analysis of the ratio of (l) H3K4me2:H3K27me3 and (m) H3K27me3:H3K4me2
1099 enrichment at the *Myh11* locus in AA vSCs in the absence or presence of rSHh (0.5 µg/ml)
1100 with or without cyclopamine (10µM) for 7 d.

1101 **n**. Fold enrichment of H3K4me2 at the *Myh11* locus in AA vSCs in the absence or presence of
1102 rSHh (0.5 µg/ml) with or without cyclopamine (15µM) for 7 d. Fresh aortic tissue and mouse
1103 ECSs was used as positive and negative controls, respectively Data are the mean ± SEM, n=3,
1104 #p≤ 0.05 versus aorta/ESC, *p≤ 0.05 vs vSC, §p≤ 0.05 vs rSHh.

1105 **o.** Representative immunocytofluorescence staining and **p.** the fraction of Cnn1 and Myh11
1106 positive cells in the absence or presence of rSHh (0.5 µg/ml) with or without cyclopamine
1107 (15µM) for 7 days. Representative images shown, Scale bar = 50 µm. Cumulative data is the
1108 mean ± SEM, n=3, #p≤ 0.05 versus control, *p≤ 0.05 vs rSHh.

1109

1110 **Figure 6. Human neuroectoderm progenitors express S100β cells and are present in vascular**
1111 **lesions**.

1112 **a.** Representative phase contrast photomicrographs, hematoxylin and eosin (H&E) staining,
1113 DAPI staining (blue) and immunocytochemical staining for smooth muscle cell α-actin (SMA)
1114 (red), S100β (red) and PTCH1 as indicated in the adventitial (A), medial (M), and intimal (I)
1115 sections of normal human and arteriosclerotic arteries. Scale bar=50µm. Data are
1116 representative of 3 sections from 3 patient cohorts.

1117 **b.** Phase contrast images, fluorescence staining of DAPI nuclei (blue) and
1118 immunoctytochemical analysis of the expression of OCT4 (green), S100β (green) in NEPs and
1119 CNN1 (green) and MYH11 (green) in NEP-derived SMCs. All cells were generated as described
1120 previously [43]. Scale bar = Right panels: 50µm, Left panels: 20µm. Data are representative of
1121 five images per experimental group from three independent cultures.

1122 **c.** The fraction of S100β, $CNN1^+$ and $MYH11^+$ cells in HiPSCs, NEPs and NEP-SMCs. Data are
1123 mean ± SEM, n=3, #p≤ 0.05 versus HiPSCs.

1124 **d.** Relative levels of S100β, CNN1 and MYH11 in HiPSCs, NEPs and NEP-SMCs, respectively.
1125 Data are expressed as the Log2 fold change in mRNA levels relative to HiPSCs in culture and
1126 are the mean ± SEM, n=3, #p≤ 0.05 versus HiPSCs.

1127 **e,f.** Relative levels of **(e)** CNN1 and (**f)** MYH11 in NEPs in the absence or presence of hSHh
1128 (0.5µg/ml) with or without cyclopamine (10µM) for 12 d. Data are representative of three
1129 independent cultures, #p≤ 0.05 versus NEPs, *p≤ 0.05 vs hSHh.

1130 **g.** Immunoctytochemical analysis of CNN1 (green) expression and DAPI (blue) staining in NEPs
1131 in the absence or presence of recombinant hSHh (0.5 µg/ml) for 12 d. Data are representative
1132 of five images per experimental group from two independent cultures.

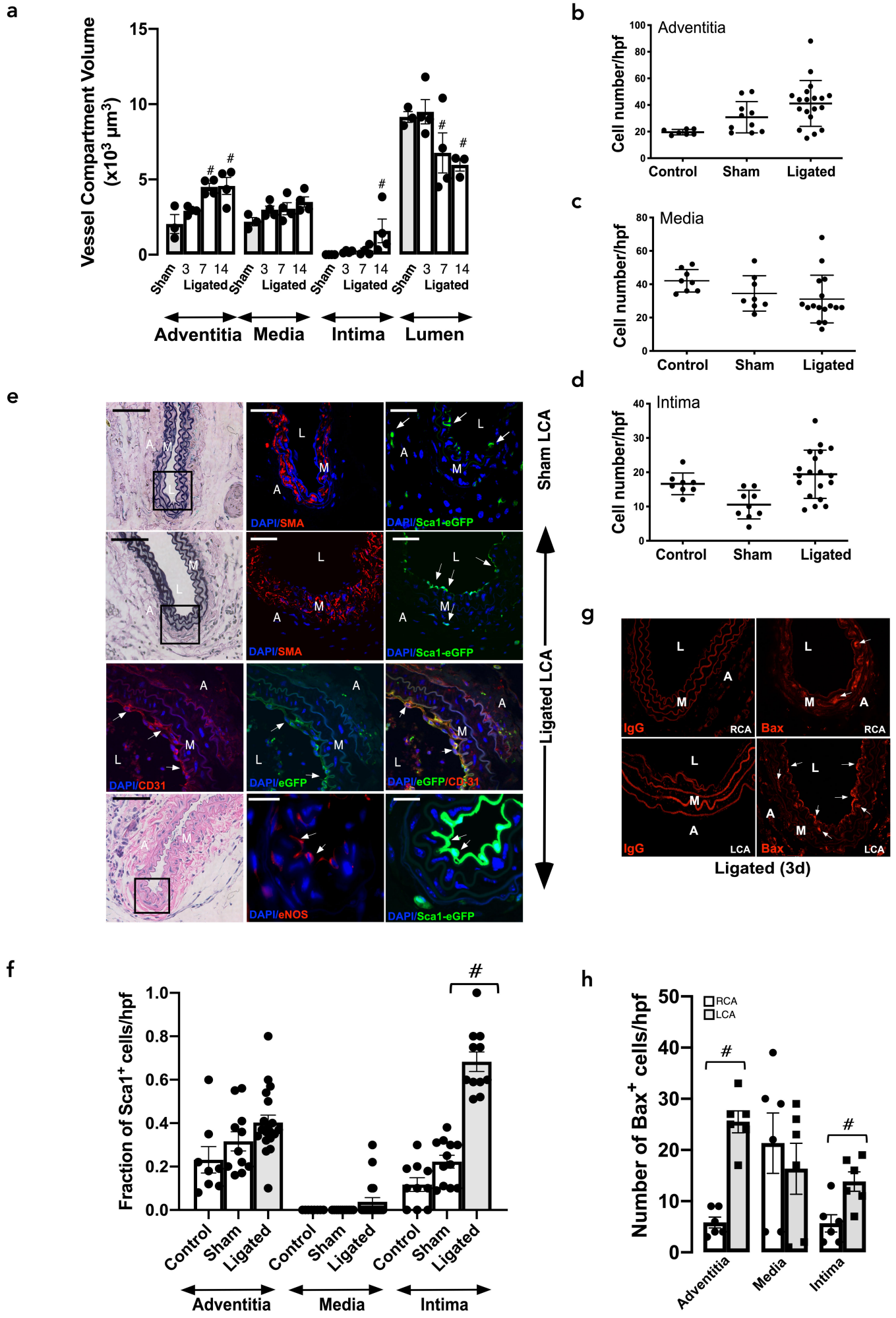
a
Vessel Compartment Volume (x10³ µm³)
Sham
3 7 14
Ligated
Adventitia
Media
Intima
Lumen
b
Adventitia
Cell number/hpf
Control
Sham
Ligated
c
Media
d
Intima
e
Sham LCA
Ligated LCA
DAPI/SMA
DAPI/Sca1-eGFP
DAPI/CD31
DAPI/eGFP
DAPI/eGFP/CD31
DAPI/eNOS
g
IgG
Bax
RCA
LCA
Ligated (3d)
f
Fraction of Sca1⁺ cells/hpf
h
Number of Bax⁺ cells/hpf
RCA
LCA

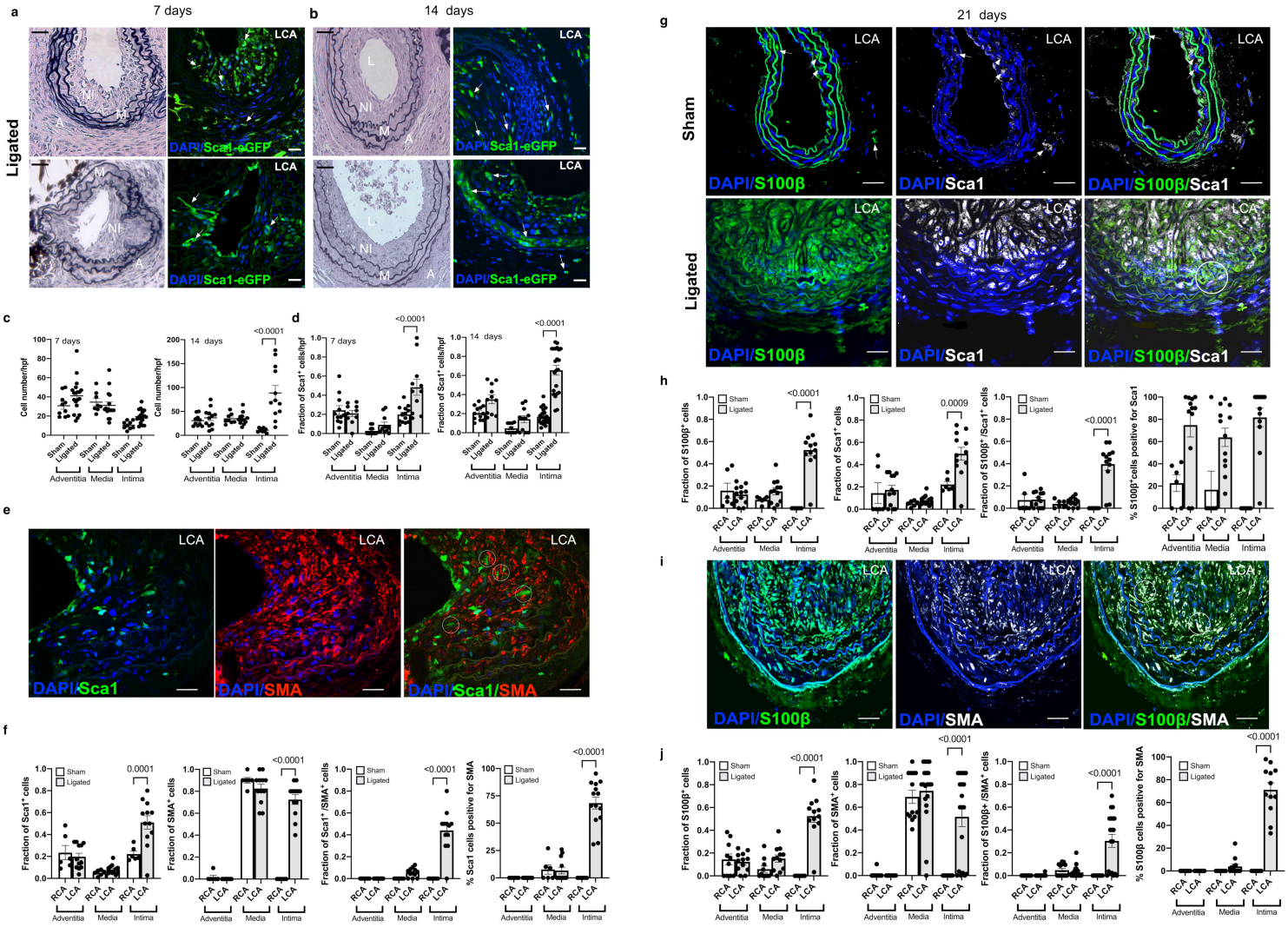
a
7 days
b
14 days
Ligated
LCA
DAPI/Sca1-eGFP
L
NI
M
A
c
7 days
14 days
Cell number/hpf
<0.0001
Sham
Ligated
Adventitia
Media
Intima
d
Fraction of Sca1+ cells/hpf
e
DAPI/Sca1
DAPI/SMA
DAPI/Sca1/SMA
f
Fraction of Sca1+ cells
Fraction of SMA+ cells
Fraction of Sca1+/SMA+ cells
% Sca1 cells positive for SMA
0.0001
RCA
LCA
g
21 days
Sham
DAPI/S100β
DAPI/Sca1
DAPI/S100β/Sca1
h
Fraction of S100β+ cells
Fraction of Sca1+ cells
Fraction of S100β+/Sca1+ cells
% S100β+ cells positive for Sca1
0.0009
i
DAPI/S100β
DAPI/SMA
DAPI/S100β/SMA
j
Fraction of S100β+ cells
Fraction of SMA+ cells
Fraction of S100β+/SMA+ cells
% S100β cells positive for SMA

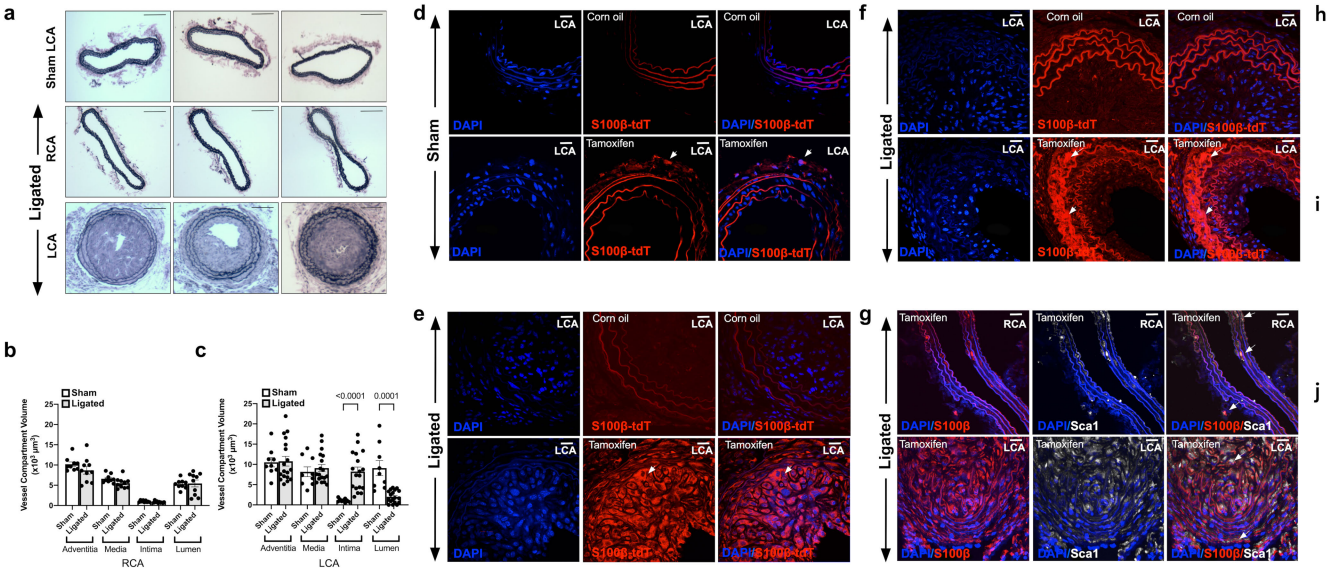
a
Sham LCA
RCA
LCA
Ligated
b
Sham
Ligated
Vessel Compartment Volume (x10³ µm³)
Adventitia
Media
Intima
Lumen
RCA
c
<0.0001
0.0001
LCA
d
Sham
Corn oil
Tamoxifen
DAPI
S100β-tdT
DAPI/S100β-tdT
e
Ligated
f
g
DAPI/S100β
DAPI/Sca1
DAPI/S100β/Sca1
h
Fraction of S100β-tdT⁺ cells
0.0001
i
0.0193
<0.0001
j
Fraction of Sca1/S100β-tdT⁺ cells
0.0673
<0.0001

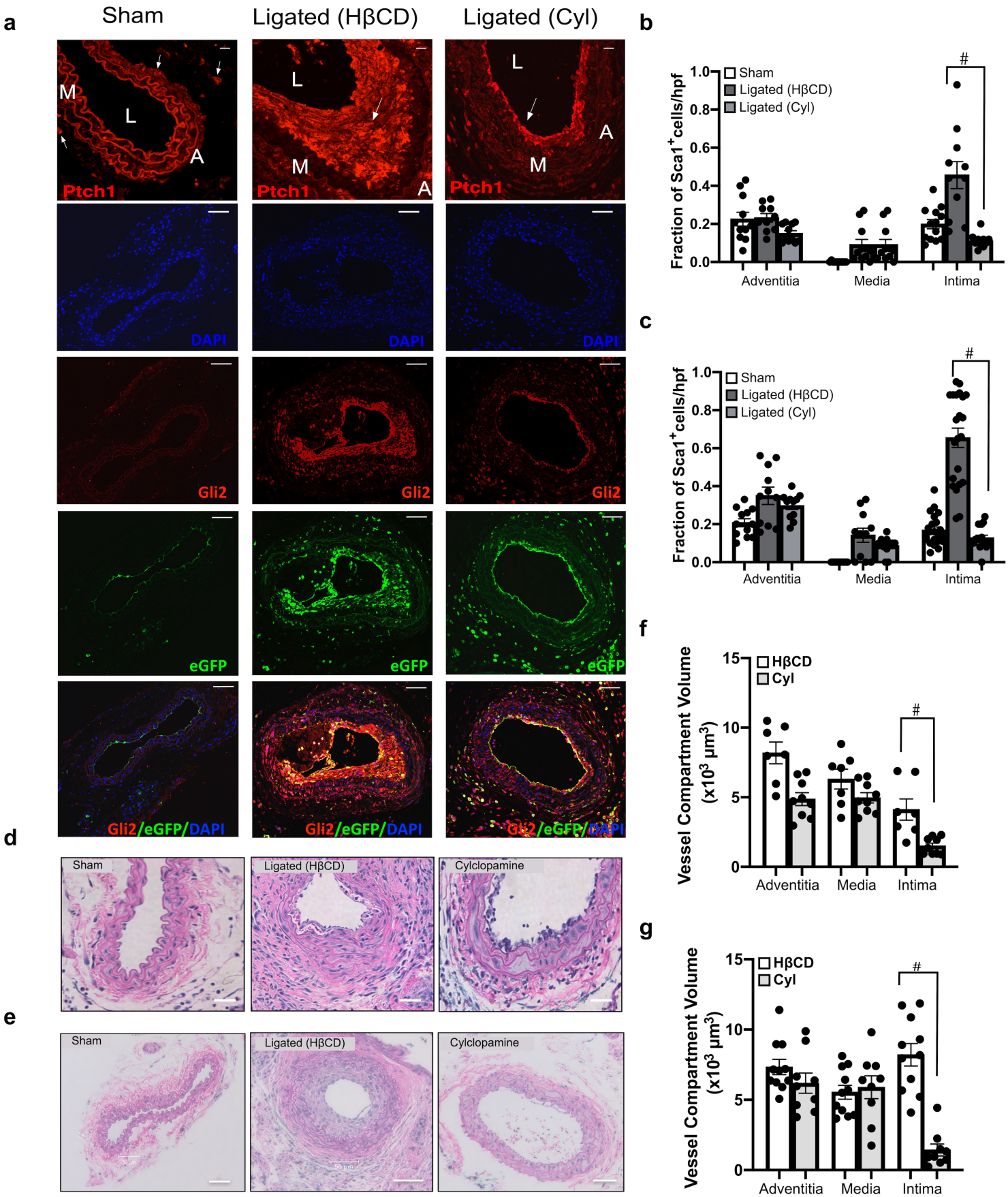
a
Sham
Ligated (HβCD)
Ligated (Cyl)
M
L
A
Ptch1
DAPI
Gli2
eGFP
Gli2/eGFP/DAPI
b
Fraction of Sca1+cells/hpf
Sham
Ligated (HβCD)
Ligated (Cyl)
Adventitia
Media
Intima
#
c
Fraction of Sca1+cells/hpf
Sham
Ligated (HβCD)
Ligated (Cyl)
Adventitia
Media
Intima
#
d
Sham
Ligated (HβCD)
Cyclopamine
e
Sham
Ligated (HβCD)
Cyclopamine
f
Vessel Compartment Volume (x10³ µm³)
HβCD
Cyl
Adventitia
Media
Intima
#
g
Vessel Compartment Volume (x10³ µm³)
HβCD
Cyl
Adventitia
Media
Intima
#

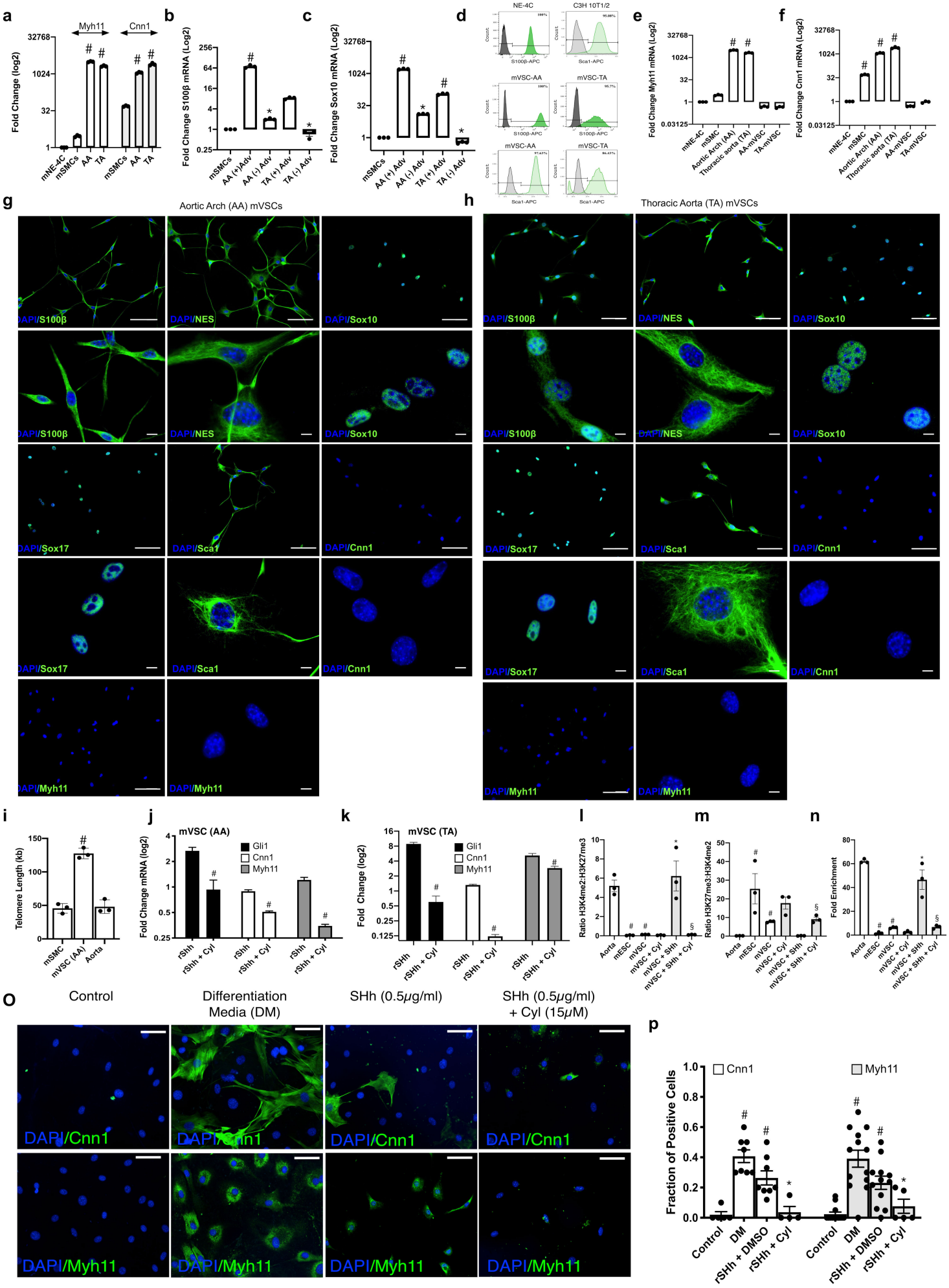
a
Myh11
Cnn1
Fold Change (log2)
mNE-4C
mSMCs
AA
TA
b
Fold Change S100β mRNA (Log2)
mSMCs
AA (+) Adv
AA (-) Adv
TA (+) Adv
TA (-) Adv
c
Fold Change Sox10 mRNA (Log2)
d
NE-4C
C3H 10T1/2
mVSC-AA
mVSC-TA
S100β-APC
Sca1-APC
e
Fold Change Myh11 mRNA (Log2)
Aortic Arch (AA)
Thoracic aorta (TA)
AA-mVSC
TA-mVSC
f
Fold Change Cnn1 mRNA (Log2)
mSMC
g
Aortic Arch (AA) mVSCs
DAPI/S100β
DAPI/NES
DAPI/Sox10
DAPI/Sox17
DAPI/Sca1
DAPI/Cnn1
DAPI/Myh11
h
Thoracic Aorta (TA) mVSCs
i
Telomere Length (kb)
mSMC
mVSC (AA)
Aorta
j
mVSC (AA)
Fold Change mRNA (log2)
Gli1
Cnn1
Myh11
rShh
rShh + Cyl
k
mVSC (TA)
Fold Change (log2)
l
Ratio H3K4me2:H3K27me3
mESC
mVSC
mVSC + Cyl
mVSC + SHh
mVSC + SHh + Cyl
m
Ratio H3K27me3:H3K4me2
n
Fold Enrichment
o
Control
Differentiation Media (DM)
SHh (0.5μg/ml)
SHh (0.5μg/ml) + Cyl (15μM)
DAPI/Cnn1
DAPI/Myh11
p
Fraction of Positive Cells
Cnn1
Myh11
Control
DM
rSHh + DMSO
rSHh + Cyl

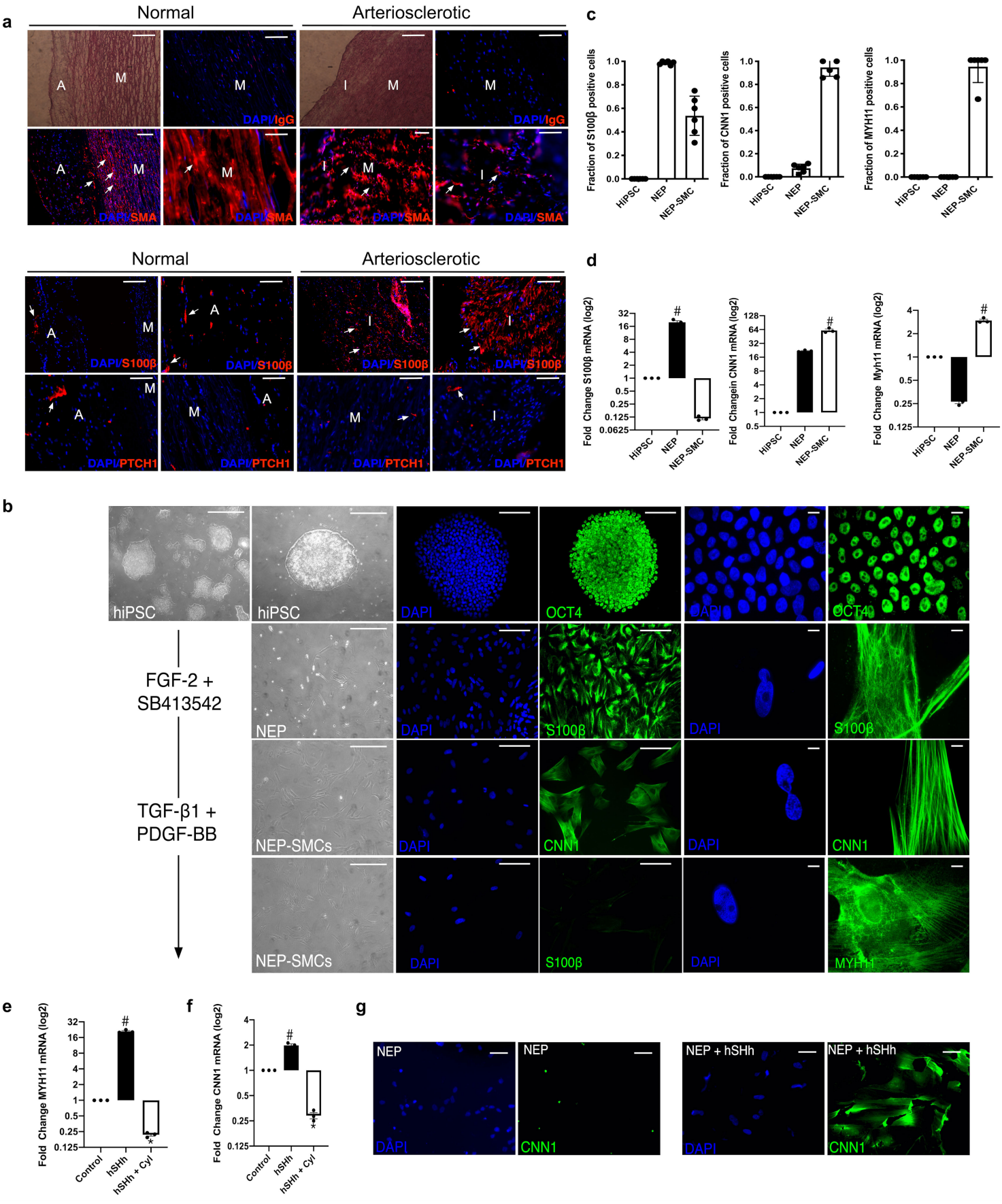
a
Normal
Arteriosclerotic
A
M
I
DAPI/IgG
DAPI/SMA
DAPI/S100β
DAPI/PTCH1
c
Fraction of S100β positive cells
Fraction of CNN1 positive cells
Fraction of MYH11 positive cells
HiPSC
NEP
NEP-SMC
d
Fold Change S100β mRNA (log2)
Fold Changein CNN1 mRNA (log2)
Fold Change Myh11 mRNA (log2)
#
b
hiPSC
DAPI
OCT4
FGF-2 +
SB413542
NEP
S100β
TGF-β1 +
PDGF-BB
NEP-SMCs
CNN1
MYH11
e
Fold Change MYH11 mRNA (log2)
Control
hSHh
hSHh + Cyl
f
Fold Change CNN1 mRNA (log2)
g
NEP + hSHh